Advanced Fiber Materials (2024) 6:1053–1073
https://doi.org/10.1007/s42765-024-00397-6

RESEARCH ARTICLE

# Electrospun trilayer eccentric Janus nanofibers for a combined treatment of periodontitis

**Ping Zhao[1] · Kecong Zhou[2,3,4] · Yiru Xia[2,3,4] · Cheng Qian[5] · Deng-Guang Yu[1] · Yufeng Xie[6,7] · Yaozu Liao[5]**

Received: 23 November 2023 / Accepted: 17 February 2024 / Published online: 12 April 2024


## Abstract

Oral diseases are common and prevalent, affecting people's health and seriously impairing their quality of life. The implantable class of materials for a safe, convenient, and comprehensive cure of periodontitis is highly desired. This study shows a proof-of-concept demonstration about the implant fibrous membranes. The fibers having a trilayer eccentric side-by-side structure are fabricated using the multiple-fluid electrospinning, and are fine candidates for treating periodontitis. In the trilayer eccentric side-by-side composite nanofibers, the outermost layer contains a hydrophilic polymer and a drug called ketoprofen, which can reach a release of 50% within 0.37 h, providing a rapid pain relief and anti-inflammatory effect. The middle layer is loaded with metronidazole, which is manipulated to be released in a sustained manner. The innermost layer is loaded with nano-hydroxyapatite, which can directly contact with periodontal tissues to achieve the effect of promoting alveolar bone growth. The experimental results indicate that the developed implant films have good wettability, fine mechanical properties, biodegradability, and excellent antibacterial properties. The implant films can reduce inflammatory responses and promote osteoblast formation by down-regulating interleukin 6 and up-regulating osteoprotegerin expression. In addition, their composite nanostructures exhibit the desired promotional effects on fibroblast attachment, infiltration, proliferation, and differentiation. Overall, the developed fibrous implant films show strong potential for use in a combined treatment of periodontitis. The protocols reported here pave a new way to develop multi-chamber based advanced fiber materials for realizing the desired functional performances through a robust process-structure-performance relationship.

**Keywords** Trilayer Janus nanofibers · Side-by-side electrospinning · Periodontitis · Combined treatment · Medical implants · Multifunctional

Ping Zhao, Kecong Zhou and Yiru Xia contributed equally to the work.

✉ Deng-Guang Yu
ydg017@usst.edu.cn

✉ Yufeng Xie
yufengxie_123@163.com

✉ Yaozu Liao
yzliao@dhu.edu.cn

[1] School of Materials and Chemistry, University of Shanghai for Science and Technology, Shanghai 200093, China

[2] Department of Periodontology, Shanghai Ninth People's Hospital, Shanghai Jiao Tong University School of Medicine, Shanghai 200023, China

[3] Shanghai Key Laboratory of Stomatology and Shanghai Research Institute of Stomatology, National Clinical Research Center for Oral Diseases, Shanghai 200023, China

[4] Shanghai Engineering Research Center of Advanced Dental Technology and Materials, Shanghai 20023, China

[5] College of Materials Science and Engineering, State Key Laboratory of Modifications On Chemical Fibers and Polymer Materials, Donghua University, Shanghai 201620, China

[6] Department of Periodontology, Shanghai Stomatological Hospital and School of Stomatology, Fudan University, Shanghai 200001, China

[7] Shanghai Key Laboratory of Craniomaxillofacial Development and Diseases, Fudan University, Shanghai 200001, China

## Introduction

With the improvements in people's living standards and changes in their dietary habits, oral health problems are becoming more and more worrying nowadays. Oral diseases are common and prevalent diseases that affect people's health. They not only affect the physiological functions of the oral cavity, such as chewing, pronunciation, and esthetics, but are also closely related to some systemic diseases, such as brain diseases [1], cardiovascular diseases [2], diabetes [3], and digestive system diseases [4], which seriously impair people's quality of life [5]. Among them, periodontal disease is one of the most harmful and prevalent dental diseases in humans [6–8]. It encompasses a group of inflammatory diseases caused by plaque, which manifests itself as a gradual destruction of the supporting tissues of teeth, resulting in the loosening or even loss of teeth [9]. At present, there are mainly surgical and non-surgical methods for the treatment of periodontitis. Comparatively, non-surgical periodontitis treatment is mainly used to eliminate inflammation and prevent the deterioration of the disease, but it has limited effect on the reconstruction and regeneration of periodontal support tissue that has been lost. Regenerative surgery is an ideal treatment for severe periodontitis because it can reconstruct the damaged periodontal tissue. Its therapeutic principle is to establish a mechanical barrier membrane to prevent epithelial and connective tissue from growing down to the defect, thereby achieving periodontal tissue regeneration, and can minimize the migration of bacteria to the deep tissue and guide bone regeneration. It should not be ignored that after implantation of the barrier film in patients with periodontitis, a large amount of local bacteria accumulation, inflammation around the material and alveolar bone absorption can be caused, resulting in loosening or loss of the barrier film [10]. Therefore, the implantable barrier membrane is highly desired for achieving periodontal tissue inflammation control or bone regeneration therapy.

However, the periodontal barrier membrane should have a series of excellent performances to support an effective, safe and comfortable tissue regeneration. Conventional materials have difficulty penetrating deep into periodontal pockets and have limited effect on the treatment of periodontitis. Electrospun fibrous membranes have exhibited their attractive potentials as medical devices for a wide variety of medical applications [11–17]. Owing to their advantages of tunable porosity, controllable morphology, strong polymer processing capability, huge specific surface area and high flexibility, the traditional electrospun mono-axial homogeneous nanofibers from the single-fluid blending electrospinning processes have been reported to be useful in treating periodontitis [18, 19]. However, electrospinning is rapidly moving forward to the multi-fluid processes for creating multi-chamber nanostructures [20, 21]. These complex structures are facile in tailoring components, compositions, and spatial distributions within the electrospun nanofibers, and thus are powerful for providing multiple functional performances or realizing the designed synergistic action [22–25]. It can be hypothesized that the electrospun heterogeneous nanofibers with multi-chamber nanostructures are facile to be loaded with multiple active ingredients with each has its favorite release profile for a synergistic therapy, and thus can meet the requirements for a comprehensive treatment of periodontitis [26–28]. Electrospinning and electrospraying have the advantages of easy interaction between fluids and electrostatic energy for nanofabrication [27–29]. The resultant electrospun fibrous membranes have a physical structure similar to the extracellular matrix (ECM). Their unique properties, such as high specific surface area and fine permeability, are able to provide a favorable environment for cell adhesion and proliferation, and have been explored as novel scaffold materials for guiding tissue regeneration [30–33]. To date, most of the investigations are based on electrospun monolithic composites fabricated from a single-fluid blending process [34], based on which multiple-fluid electrospinning processes are continuously developed for creating a series of complicated nanostructures, such as core–shell, Janus, trilayer core–shell, and combinations of core–shell and Janus nanostructures [35–37]. These multiple-chamber nanostructures can be facilely exploited to tailor their components, compositions, and spatial positions within the nanoscale, which, in turn, provides a powerful tool for developing novel multiple-functional nanodevices. Accordingly, it can be hypothesized that these multiple-compartment fibrous films can be explored to deliver several active ingredients simultaneously and controllably to periodontal pockets to promote tissue regeneration, prevent infection, and, in turn, achieve a combined treatment of periodontitis.

Based on the properties of their polymers, periodontal implant films are divided into non-absorbable and absorbable films [38]. Environmentally friendly implant membranes with biodegradable properties that avoid the destruction of de novo tissues and reduce the risk of infection are gradually being used as periodontal regenerative implant membranes. In the existing literature, polycaprolactone (PCL), poly(lactic-co-glycolic acid) (PLGA), polylactic acid (PLA), chitosan (CS), and gelatin (Gel) have been proposed as candidates for electrospun scaffolds [5, 39–42]. Among them, the weaker mechanical properties and poor spinnability and stability limit the use of natural-type polymers (e.g., CS and Zein) [43]. By contrast, synthetic polymers such as PCL have many advantages such as good biocompatibility, excellent mechanical properties, filament formation,

and biodegradability; especially since they do not produce a local acidic environment when degraded, these synthetic polymers make ideal implant materials for periodontitis treatment [44]. However, it should not be overlooked that PCL is also extremely hydrophobic, which is not conducive to drug release for wound healing. Therefore, the addition of the soluble polymer polyvinylpyrrolidone (PVP) can, on the one hand, enhance the rapid release of insoluble drugs and, on the other hand, enhance the hydrophilicity of nanofiber membranes to promote a rapid wound healing process.

Currently, the antibacterial properties of metronidazole (MET), amoxicillin (AMX), ciprofloxacin (CIP), and minocycline (MINO) [45–48]; the anti-inflammatory properties of ibuprofen (IBU) and meloxicam (MX) [49, 50]; and the osteogenic properties of zinc oxide nanoparticles (ZnO), hydroxyapatite nanoparticles (nHA), and silicon oxide nanoparticles (nSi) [51–53] have been demonstrated using uniaxial blending electrospinning. Since it is difficult to achieve simultaneous anti-inflammatory, antibacterial, and bone regeneration therapeutic effects with a single drug, a combination therapy with the synergistic effects of multiple active ingredients would be a better option to cure periodontitis.

In this investigation, multifunctional complex nanofiber implant membranes with a trilayer eccentric side-by-side structure were designed and fabricated in one step using a trifluid side-by-side electrospinning process, with PCL as the main filament-forming matrix and PVP as the auxiliary polymer. The outermost layer is loaded with KET to reduce tissue inflammation by inhibiting the activity of cyclooxygenase (COX). The middle layer is loaded with MET to prevent bacterial colonization in the epithelial tissue for antibacterial effect. The innermost layer is loaded with nHA to enhance the formation of bone tissue at the bone defect. To the best of our knowledge, this study is the first to prepare nanofiber implant membranes with a trilayer eccentric side-by-side structure using multiple-fluid electrospinning, and it is also the first study to prepare a multifunctional composite nanofiber material by loading three active substances with different efficacies into three chambers in a single step. The nanofiber implant membranes prepared in this research not only have enhanced flexibility, hydrophilicity, degradability, and mechanical performances, but also a high special surface area to improve protein uptake, intracellular signaling, and cell adhesion, to promote specific gene expression, and to accelerate coagulation. Meanwhile, their porous structure and micro-nanometer diameter can mimic the natural extracellular matrix and effectively prevent fibroblasts from crossing the barrier membrane, thus providing a potential ideal material for the combined treatment of periodontitis.

## Experimental section

### Materials

Polycaprolactone (PCL, $M_n = 80{,}000$), ketoprofen (KET, $M_n = 254.29$), metronidazole (MET, $M_n = 171.15$), nanohydroxyapatite (nHA, $M_n = 502.31$), polyvinylpyrrolidone (PVP K30, $M_n = 40{,}000$), 2,2,2-Trifluoroethanol ($CF_3CH_2OH$, TFE, $M_n = 100.04$), and phosphate-buffered solution (PBS, pH = 7.0 and pH = 8.4) were obtained from Sigma-Aldrich Co., Ltd. (Shanghai, Vina). A Porphyromonas gingivalis strain (*P.g*, ATCC 33277), human gingival fibroblasts (HGFs), the medium DMEM, dual antibodies (penicillin and streptomycin), RNA Trizol, a real-time fluorescent light quantitative reverse transcription PCR kit, a qPCR kit, CCK8 reagent, an IL-6 kit, an OPG kit, a Calcein/PI cell activity and cytotoxicity assay kit, P. gingivalis LPS, and brain heart infusion broth were bought from Shanghai Hao-Sheng Biotechnology Co., Ltd. (Shanghai, China). Water was doubly distilled just before usage.

### Preparation of implanted fibrous membrane

As shown in Fig. 1, the electrospinning system used in this study consisted of a homemade trilayer eccentric side-by-side spinneret (the details about the spinneret are shown in Fig. S1 in the Supplementary Materials), a DC high-voltage generator (ZGF2000 60 kV/2 mA), a receiver unit, and three KDS100 fluid drivers (Cole-Parmer, Vernon Hills, IL, USA). Blank group fibers, uniaxial drug-carrying fibers, and tri-layer side-by-side composite nanofibers were prepared using TFE as a solvent to dissolve the polymers and drugs.

Some primary experiments were conducted on the electrospinnability of different kinds of working fluids (the SEM images of the resultant nanofibers are shown in Fig. S2 to Fig. S6 in the Supplementary Materials). The working fluids for preparing the PCL nanofibers and PCL nanofibers loaded with three different types of drugs are listed in Table 1. The preparation of the trilayer Janus F4 nanofibers was carried out by slightly reducing the polymer concentrations, thereby providing a smooth and continuous multiple-fluid working condition due to a reduction in the interfacial tensions among the three working fluids. The fiber deposition distance was fixed at 18 cm. The fluid flow rates for preparing the F0 to F3 nanofibers were kept at 0.9 mL/h during the single-fluid electrospinning process. A flow rate of 0.3 mL/h was exploited for the three working fluids during the trifluid side-by-side electrospinning process. The applied voltages were adjusted

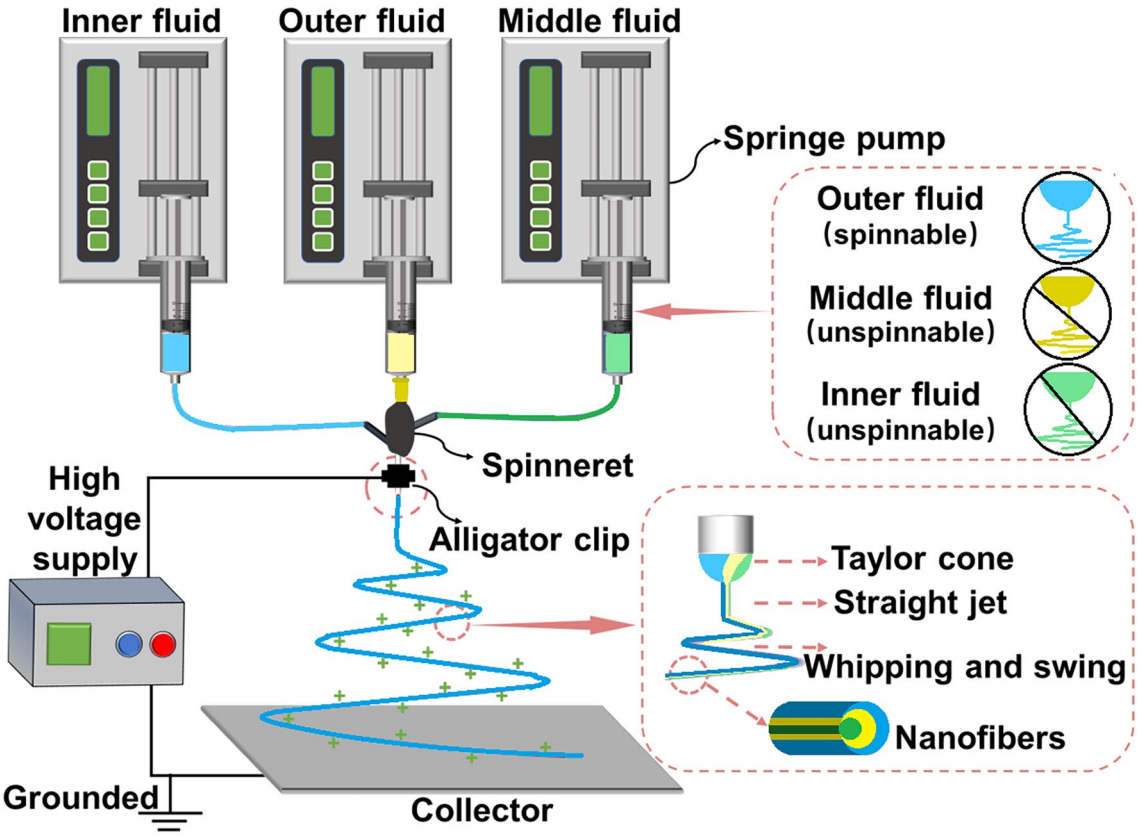


**Fig. 1** Tri-layer eccentric side-by-side electrospinning system

**Table 1** Experimental parameters for preparing different kinds of nanofibers

| No | Working process | Applied Voltage (kV) | Outer-side fluid [a] | | | Middle-side fluid[a] | | Inner-side fluid[a] | |
|---|---|---|---|---|---|---|---|---|---|
| | | | PCL | KET | PVP | PCL | MET | PCL | nHA |
| F0 | Single | 8.0 | 1.4 | – | – | – | – | – | – |
| F1 | Single | 8.0 | 1.4 | 0.2 | 0.2 | – | – | – | – |
| F2 | Single | 8.0 | – | – | – | 1.4 | 0.2 | – | – |
| F3 | Single | 12.0 | – | – | – | – | – | 1.4 | 0.2 |
| F4 | Trifluid side-by-side | 12.0 | 1.4 | 0.2 | 0.2 | 1.2 | 0.2 | 1.0 | 0.2 |

[a]The unit of component concentration is g·10/mL and the solvent is TFE

The symbol "–" represents none

to make the electrospinning reach a steady and continuous state and are listed in Table 1. All experiments were carried out under an ambient temperature of 25 ± 3 °C and a relative humidity of 45 ± 5%.

## Morphological and structural characteristics of nanofibers

A small portion of the prepared nanofibers was cut and attached to the sample stage with conductive adhesive, and the sample was sputtered for 90 s using a gold rod under a nitrogen atmosphere. The morphologies of the nanofibers were evaluated using a field-emission scanning electron microscope (SEM) (Quanta FEG 450, FEI, Hillsboro, OR, USA). One hundred randomly selected fibers were sampled based on the SEM's graph, and fiber diameters were measured using ImageJ software (National Institutes of Health, Bethesda, USA). The distribution of elements in the trilayer Janus nanofibers was analyzed and determined using an energy-dispersive X-ray spectrometer (EDX) (Tecnai G2 F30, FEI, Hillsboro, OR, USA). The nanofibers were collected using a 200-mesh copper mesh and dried overnight in a drying dish, and the internal

structure of the nanofibers was evaluated using transmission electron microscopy (TEM) (Tecnai G2 F30, FEI, Hillsboro, OR, USA).

## Contact angle test and swelling rate test

The surface wettability of the nanofibers was tested using a contact angle meter (Power each, Shanghai Zhongchen Digital Technology Equipment Co., Ltd., China). The samples were cut into rectangles of 30 mm × 10 mm with uniform thickness, pressed onto glass slides, and placed on a working table. The liquid in the probe was 3.0 μL of distilled water. The change process of water droplets was observed at different time points, and each experiment was repeated six times.

The water absorption capacity of the nanofibers was tested with reference to the Pharmaceutical Industry Standard of the People's Republic of China, YY/T 0471.1–2004 "Test Method for Contact Wound Dressings Part 1: Liquid Absorption", and the nanofibers were cut into squares of 20 mm × 20 mm with a thickness of about 0.1 ~ 0.25 mm, weighed with a balance, and the initial mass was recorded as $W_D$. The weighed samples were placed in phosphate-buffered saline (PBS, pH = 7.0) at a constant temperature of 37℃ for 24 h. The samples were collected and excess water was gently removed using filter paper. At this point, the weight of the samples was recorded as $W_W$ and the water absorption Q (%) of the nanofibers was calculated using the equation below (Eq. 1). Six replicate tests were performed for each sample, and the results are reported as mean ± standard deviation.

$$Q(\%) = \frac{W_W - W_D}{W_D} * 100 \quad (1)$$

## Mechanical property test

The middle part of the trilayer Janus nanofibers with similar thickness was selected and cut into 50 mm × 20 rectangular pieces; three different positions were selected to measure the thickness using a spiral micrometer, and the average value was taken as the final result of the measured thickness. The mechanical properties of the nanofibers were tested using a microtensile testing machine (Precision Line Vario, Zwick, Germany), which was pulled at a fixed speed of 1.0 mm/min. The test results are reported as the corresponding tensile strength, elongation at break, and Young's modulus. The test was repeated six times for each sample, and the results are reported as mean ± standard deviation.

## Fiber membrane degradability test

Each group of fibrous membranes was cut into 12 squares of similar thickness with a size of 20 mm × 20 mm, and the initial mass was recorded as $W_0$ in two groups. Each group of six membranes was placed in different 150 mL conical flasks with PBS (pH = 7.0 or pH = 8.4) and incubated in a shaker under the following conditions: water bath shaking, 37 °C, and 50 rmp. The membranes were first rinsed with distilled water to remove any remaining surface materials, and then filter paper was used to absorb excess water. The membranes were then kept at room temperature for 24 h to dry to ensure that they were in a dry state, and after water had completely evaporated, the membranes were weighed using a microbalance, and the mass $W_t$ after each period of degradation was noted, using the weight loss rate (Eq. 2) to characterize the degradation capacity of the membranes. Each group of experiments was conducted six times The results are reported as the mean ± standard deviation for a period of 1 month. The calculation of the weight loss rate is as follows:

$$Weight\ loss(\%) = \frac{W_0 - W_t}{W_0} * 100 \quad (2)$$

## In vitro drug dissolution tests

In vitro dissolution tests were performed according to the paddle method described in the *Chinese Pharmacopoeia* (2020 Ed.). An amount of 100 mg of nanofibers containing the drug being tested was immersed in 450 mL of phosphate-buffered saline (PBS, pH 7.0, 0.1 M) at 37 °C. The experiment was performed using a dissolution apparatus (RCZ-8A, Radio Factory, Tianjin University, Tianjin, China) at a temperature of 37 °C and a rotation speed of 50 rmp. At a predetermined time point, a volume of 4.0 mL of the aliquot was removed and 4.0 mL of fresh PBS was immediately added to the beaker containing the fiber membranes to maintain a constant volume. The release of KET and MET was analyzed at $\lambda_{max}$ = 260 nm and $\lambda_{max}$ = 320 nm, respectively, using an ultraviolet–visible spectrophotometer (UV-2102PC, Shanghai United Instruments Co., Ltd., China). The experiments were repeated six times for each samples, and the accumulative percentages of released drug from the fibers were calculated using a calibration curve (Eq. 3). All the results are reported as mean ± standard deviation. To avoid the mutual influence of two drugs, two additional patches of trilayer F4 nanofibers were prepared, and only one drug of either KET (denoted as F4-KET) or MET (denoted as F4-MET) was loaded in them. The calculation of the cumulative percentage of each drug is as follows:

$$P(\%) = \frac{C_n * V_0 + \sum_{i=1}^{n-1} C_i * V}{Q_0} * 100 \quad (3)$$

where $V_0$ is the volume of the dissolution medium (450 mL), $V$ is the volume of the sample drawn (4 mL), $Q_0$ is the

theoretical amount of the drug in each sample (mg), $C_n$ is the concentration of the drug measured in the nth aliquot (mg/L), and $C_i$ is the concentration of the drug in the i-th aliquot (mg/L).

## Antibacterial experiment

The antimicrobial properties of the F0 ~ F4 nanofiber membranes were studied using the paper diffusion method. A total of 100 L of the liquid culture containing $1 \times 10^6$ CFU of *P.g* strain of each microorganism was spread on nutrient agar plates. The nanofiber membranes were then cut into 6 mm discs and sterilized with UV light for 2 h. The discs were applied to the surface of the agar plates using sterile forceps and incubated in a constant-temperature incubator at 37 °C. After 48 h of anaerobic incubation, the size of the diameter of the inhibition zone around the discs and the bacterial activity were measured. Each group of experiments was repeated six times, and the results are reported as mean ± standard deviation.

## Cell culture

The removed human gingival tissue was washed with PBS (pH = 7.0) to remove residual blood and secretions, and the tissue was cut into small pieces and immediately placed in DMEM containing 1% penicillin/streptomycin and 10% fetal bovine serum to prepare a cell suspension. The cell suspension was evenly distributed into the culture flasks so that it adhered evenly to the surface of the flasks. The culture flasks were placed in an incubator with constant temperature and humidity at 37 °C and 5% $CO_2$, and primary cell culture was performed using the inverted tissue block method. When cells were observed to be attached to the culture flasks and the number of cells had reached a sufficient number with a density of about 80%, the cells were subjected to passaged culture and cells of the 4th to 6th generations were selected for experimental manipulation.

## In vitro cytotoxicity assay

For the toxicity test of the prepared nanofibrous membranes, two experimental methods were adopted in this study: one was to add the fibrous membrane material to the cell culture medium and culture with the cells, and the other was to culture the cells on the prepared nanofibrous material until they adhered to the fiber surface, and then the cells were washed with appropriate buffers to remove the culture medium and impurities. The cells after the above treatment were stained for live/dead cells according to the instructions of the staining kit, and after staining, the cells were placed under a fluorescent microscope for observation and photographic recording. Based on parameters such as color, intensity, and distribution of fluorescence, the living and dead statuses of the cells were judged.

## Cell proliferation and adhesion

Cell proliferation was studied using the cell counting assay (CCK-8). HGFs were inoculated in 96-well plates with different nanofibers, and the control group consisted of cells cultured without nanofibers. The samples were incubated in a medium with 10% CCK-8 solution at 37 °C and under 5% $CO_2$ atmosphere for 24 h. The optical density (OD) values at 450 nm were read using an enzyme marker after 1, 3, 5, and 7 days.

Sterilized specimens were placed into each well of a 24-well tissue culture plate. Then, cells at a density of $1 \times 10^5$ cells/mL were inoculated onto the samples and incubated at 37 °C and 5% $CO_2$ in a humid atmosphere for 24 h. After cell adhesion, a certain amount of the medium containing 10% fetal bovine serum was added to each well. One day later, the medium was removed from the specimens, which were washed with phosphate-buffered saline for 30 s. Cells were fixed with 3.5% glutaraldehyde and then dehydrated with increasing concentrations of ethanol. Finally, cell adhesion to the specimens was observed via scanning electron microscopy.

## Inflammation and osteogenic gene expression

Cells can be tested for in vitro gene expression using the polymerase chain reaction technique. Sterilized specimens were first placed in each well of a 24-well tissue culture plate. Cells at a density of $1 \times 10^5$ cells/mL were then inoculated onto the samples and incubated at 37 °C and 5% $CO_2$ in a humid atmosphere for 24 h. Cells at a density of $10^5$ cells/mL were then inoculated in a 6-well plate, and incubation continued for 4 h with the blank culture medium or the culture medium containing LPS (polysaccharide). The cell samples were lysed using the TRIzol kit, and total RNA was extracted. cDNA was then transcribed from the extracted RNA using reverse transcriptase and random primers. The cDNA template, specific primers, heat-stable DNA polymerase, and other reagents were added to the PCR amplification kit, and the reaction system was placed in the PCR instrument for PCR amplification reaction to obtain IL-6 gene amplification products. The PCR amplification products were subjected to electrophoresis, and the success of IL-6 gene amplification was checked by examining the electrophoresis results. The qPCR tool was used to convert the PCR results into quantitative results for analysis. The expression of the osteogenic gene OPG was detected by using the same method.

### Statistical analysis

All data are expressed as mean ± standard deviation (S.D.). One-way ANOVA (Origin 8.5 software, Northampton, Massachusetts, USA) was performed, and different letters indicate differences between groups ($P < 0.05$).

## Results and Discussion

### Trilayer side-by-side eccentric electrospinning

Firstly, the influence of flow rate on the composite nanofibers was investigated by using different concentrations of polymers (Fig. S5). Finally, it was indicated that the nanofibers with the best morphology and the best uniformity could be obtained when the concentration in the outermost chamber was the highest and decreased from the outside to the inside. During the trifluid electrospinning process, the specific arrangement of the working fluids involved placing the spinnable solution in the outermost layer and the unspinnable solution in the middle and innermost layers. As shown in Fig. 2a, three strands of the spinning solution were loaded into three 20 mL syringes of the same size and connected to the trilayer eccentric side-by-side spinneret, the fluid driver, and the DC high-voltage power generator. It is worth noting that MET has photolysis properties, so the syringes in the middle layer were covered with aluminum foil to avoid light. The homemade trilayer eccentric side-by-side spinneret had one inlet to allow the direct insertion of a syringe containing the outermost layer of fluid. The syringes containing the middle and innermost working fluids were connected to the spinneret through the polymeric tubes, as shown in Fig. 2b. The spinneret was connected to the power supply through an alligator clip, as shown in Fig. 2c. Under the experimental conditions, a colorful Taylor cone could be observed at the tip of the spinneret with blue, red, and transparent colors for the outermost, middle, and innermost layers, respectively (as shown in the bottom-right inset of Fig. 2c, $2 \times 10^{-3}$ mg/mL of methylene blue and basic fuchsin markers were added to the outermost fluid and the middle fluid, respectively, only for visualization of the operation). The typical three-step

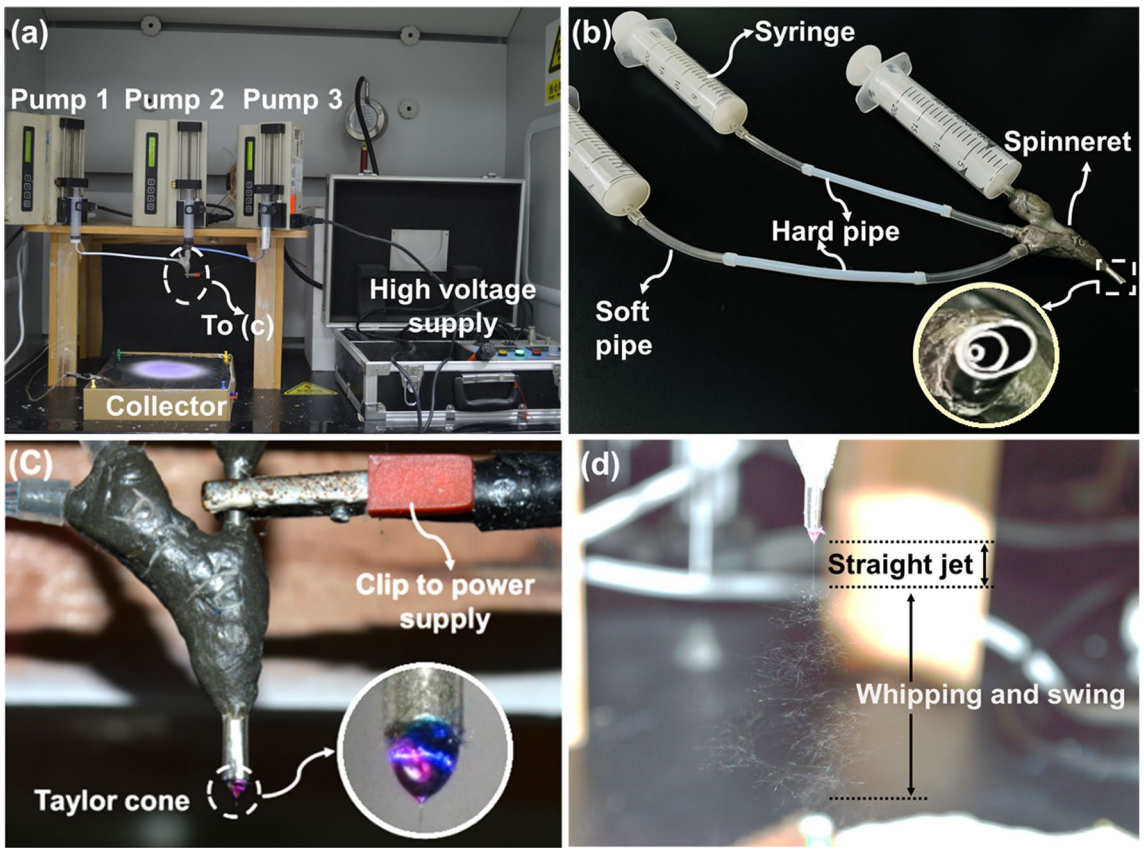


**Fig. 2** Digital images of the trilayer eccentric side-by-side electrospinning apparatus and the related working processes for creating nanofibers F4: **a** whole image of the electrospinning system, **b** the connections of the three syringes with the spinneret, with the bottom-right inset showing the trilayer eccentric co-outlet of the spinneret, **c** the connection between the spinneret and the power supply through an alligator clip, with the bottom-right inset showing a typical compound Taylor cone during the experiments, and **d** the typical straight jet and stretching whipping phenomenon during electrospinning

working processes, i.e., Taylor cone, straight fluid jet, and subsequent bending and swing instable region, are exhibited in Fig. 2d. The deposited nanofibers were dried in an oven at 40 °C for 2 h to remove the solvent from the fiber surface and stored in a sealed plastic bag in a drying dish away from light for later use.

## Fiber morphology and structure

The SEM morphology and diameter distribution of the F0 ~ F4 nanofibers are shown in Fig. 3a–e, which show that the F0, F1, and F2 nanofibers exhibit a smooth appearance without beads and each fiber is uniform in thickness. Because the F3 nanofibers are loaded with nano-hydroxyapatite, particles are sometimes formed on the surface of these fibers, and the distribution of these particles is relatively uniform. The F4 nanofibers are composite nanofibers prepared via the trilayer eccentric side-by-side electrospinning process, which show a smooth and bead-free structure. The size distribution and average diameter of these structured nanofibers were analyzed using ImageJ software, and the results showed that the F2 nanofibers showed the largest fiber diameter of $1.37 \pm 0.22$ μm, followed by the pure PCL F0 nanofibers with a diameter of $1.11 \pm 0.23$ μm, whereas the F1, F3, and F4 nanofibers had a smaller diameter of $0.38 \pm 0.08$ μm (F1), $0.36 \pm 0.06$ μm (F3), and $0.38 \pm 0.08$ μm (F4), respectively. From the results, it can be seen that nanofiber diameters decreased with drug loading except for the F2 nanofibers, probably because the addition of the drug prompted a decrease in the viscosity of the system and an increase in the conductivity of the solution, which led to a further increase in charge on the surface of the jet, resulting in the formation of smaller-diameter nanofibers due to the greater traction on the droplets [54]. To investigate the loading of nHA on the composite fibers, the F4 nanofibers were tested using an energy spectrometer. The results (Table S1 in the Supplementary Materials) demonstrated that the F4 nanofibers contained P and Ca in addition to C, N, and O elements, proving that nHA particles had been successfully loaded into the F4 nanofibers.

The internal structure of the F4 nanofibers was probed using TEM under an applied voltage of 300 keV, and the results are shown in Fig. 3f. The F4 nanofibers showed a clear trilayer Janus structure, in which the outermost, middle,

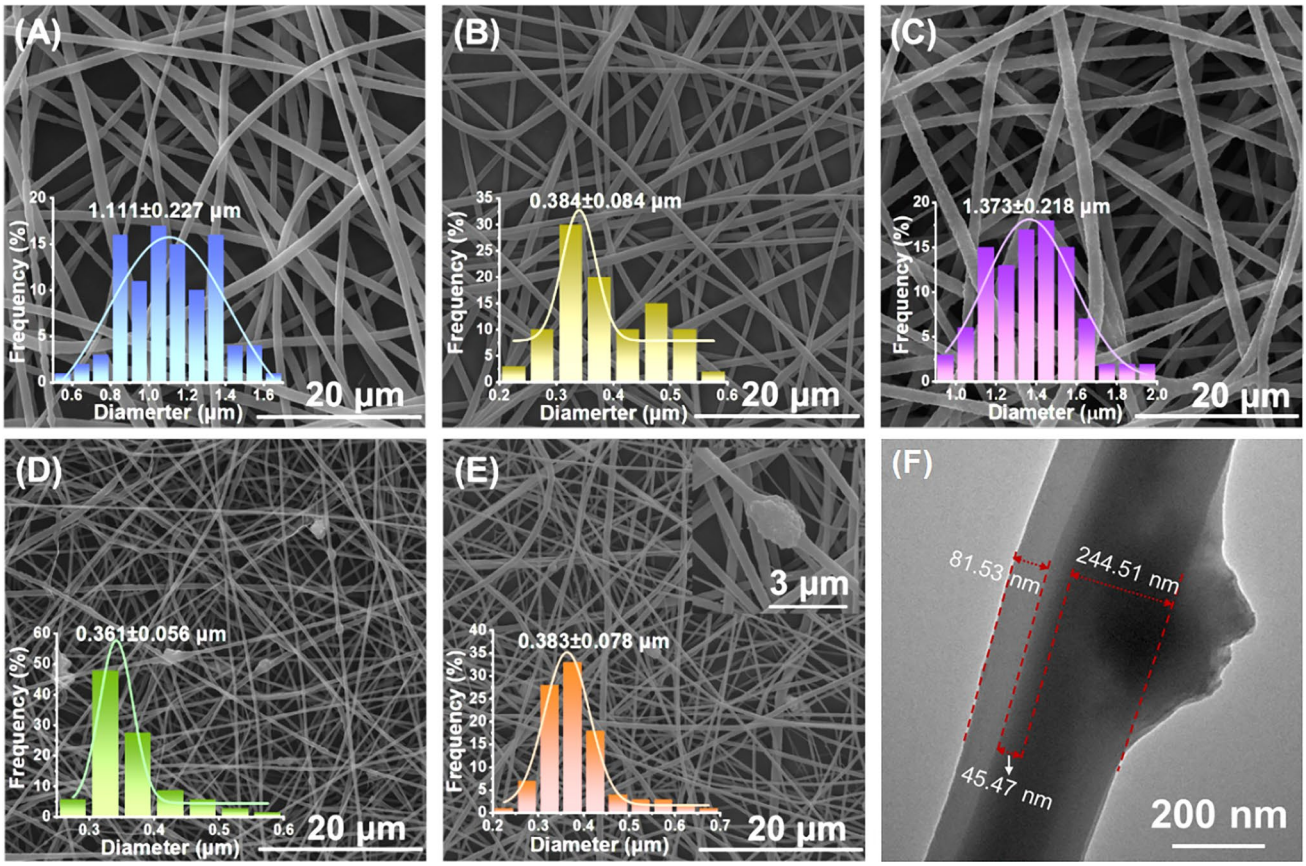


**Fig. 3** SEM images of nanofibers and their diameter distribution: **a** F0, **b** F1, **c** F2, **d** F3, and **e** F4. The up-right inset of **e** shows loaded nHA particles in F4 nanofibers. **f** TEM image of an F4 nanofiber

and innermost layers had a diameter of about 81.53, 45.47, and 244.51 nm, respectively. nHA particle loading was also found on the nanofibers, and these particles were present in the internal structure of the nanofibers. The SEM and TEM results showed that the trilayer side-by-side F4 nanofibers prepared via the multi-fluid electrospinning technique could achieve good encapsulation of drugs and successful loading of inorganic particles. These randomly oriented fibers with smaller diameters and pore sizes maintain a similar morphology to the natural extracellular matrix, which can further mimic the three-dimensional properties and structure of periodontal tissues [55]. This advantage is expected to be beneficial in promoting rapid periodontal wound healing and comprehensive treatment of periodontitis.

## Wettability and swelling rate

According to the wound healing theory, a nanofiber implant film used in periodontal wounds needs to have a certain degree of wettability to accelerate the wound healing process, and the hydrophilic properties of the implant film can be verified via the water contact angle test. The experimental results of the water contact angle of the F0 ~ F4 nanofiber membranes are shown in Fig. 4a–e). The F0 nanofibers are pure PCL nanofibers; the water contact angle of these fiber membranes hardly changed after 5 s of droplet drop and only slightly changed after 30 s, but the contact angle was still greater than 90°, which showed a strong hydrophobic property (Fig. 4a). The F1 nanofibers exhibited extremely high hydrophilicity (Fig. 4b), mainly due to the strong hydrophilicity of PVP, which contributed to the good wettability of the F1 nanofiber membrane within a very short time of water droplet shrinking. The F2 nanofibers showed hydrophobicity in the first 4 s, but their hydrophilicity gradually increased afterwards (Fig. 4c). The reasons could be attributed to the dissolution of the drug MET on the surface of the F2 nanofibers, which led to additional spreading of droplets. Although nHA is a slightly water-soluble drug, the diffusion rate of its droplets on the F3 (Fig. 4d) nanofiber membranes was slightly lower than that of the F2 nanofibers. The reason for this phenomenon may be that nHA particles are present mainly inside the F3 nanofibers, and the wettability of these internal particles only manifests when droplets have wetted the membrane surface. As for F4 (Fig. 4e) nanofibers, the instantaneous static water contact angle test results showed that the water contact angle was $90.25 \pm 1.54°$ at 50 ms and $70.36 \pm 1.06°$ at 150 ms, whereas the water contact angle of the fiber membranes was already less than 45.00° at 550 ms. The results of the water contact angle experiments showed that the composite F4 nanofibers had excellent hydrophilic properties, indicating that the trilayer eccentric side-by-side structural fibrous implants could provide an ideal physiological environment for cell growth.

A relatively moist environment can promote the absorption of wound exudate and the release of active substances at the lesion site, thus promoting wound healing. Therefore, the swelling rate of fiber membranes is an important factor to measure the metabolic function. The swelling rate test results of the F0 ~ F4 fiber membranes are shown in Fig. 4f. PCL is a hydrophobic polymer, so the swelling rate of the F0 nanofibers was low, only about $201.91 \pm 14.42\%$. The F1 nanofiber membranes exhibited a high swelling rate of approximately $472.13 \pm 32.79\%$, which was attributed to the strong hydrophilicity of PVP. The F2 and F3 nanofibers also had high swelling rates of $371.56 \pm 22.17\%$ and $390.07 \pm 28.98\%$, respectively, mainly due to the hydrophilic properties of both the drugs MET and nHA, which contributed to the water absorption properties of these nanofiber membranes. The swelling rate of the F4 composite nanofibers was second only to the F1 nanofibers, at about $431.72 \pm 28.75\%$. This indicates that the composite fibrous membrane has good swelling properties, and its high absorbency facilitates the absorption and management of wound exudate and is, thus, conducive to the promotion of wound healing.

## Mechanical properties

Periodontal implant films need to have substantial mechanical properties to meet the mechanical stresses generated by the surgical operation and the tissues in the periodontal area. Therefore, the mechanical properties of the nanofiber implant films were tested, and the results are shown in Fig. 5a. Usually, tensile strength determines the stress required to break the material, the elongation at break determines the strain required to break the material, and the modulus of elasticity determines the brittleness of the material; thus, these three parameters can be used to characterize the mechanical properties of the fiber films, and the test results are shown in Fig. 5b–d.

At the beginning of stretching, each fiber film was gradually stretched and deformed, and after a period of time, the maximum stress value was reached which then decreased rapidly, and the fiber film was completely fractured. Compared to the control group F0, the F1 and F2 nanofibers showed a significant decrease in tensile strength and elongation at break, with a decrease in tensile strength of about 34.97–35.43%, respectively, and a decrease in the elongation at break of about 59.24–85.51%, respectively, mainly due to the addition of little drug molecules in them. These fibrous membranes with different water absorption capacities and different diameter sizes also had different mechanical properties. In addition, the relative mass fraction of the fibers and polymers decreased with the addition of the drug, resulting in lower intermolecular forces and, therefore, lower tensile strength and elongation at break. The same decrease

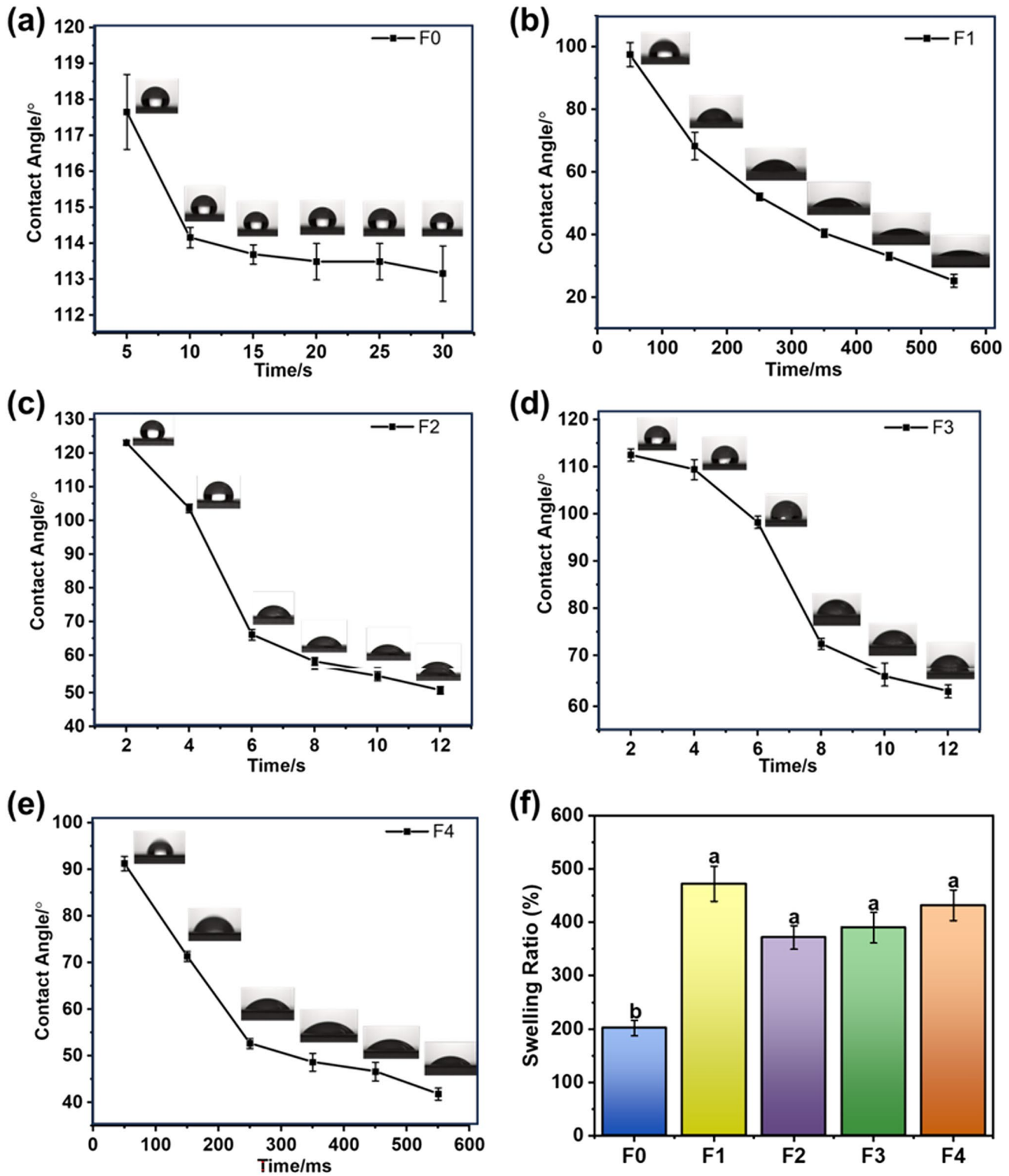


**Fig. 4** Wettability and swelling of nanofibers, showing how the static water contact angle changes with time: **a** F0 nanofiber membrane within 30 s, **b** F1 nanofiber membrane within 600 ms, **c** F2 nanofiber membrane within 12 s, **d** F3 nanofiber membrane within 12 s, **e** F4 nanofiber film within 600 ms, and **f** comparison of water swelling rates of F0-F4 nanofiber membranes over 24 h. For statistical analysis, the experimental groups F1-F4 were compared with the control group F0 (different letters indicate significant differences between groups at $P < 0.05$)

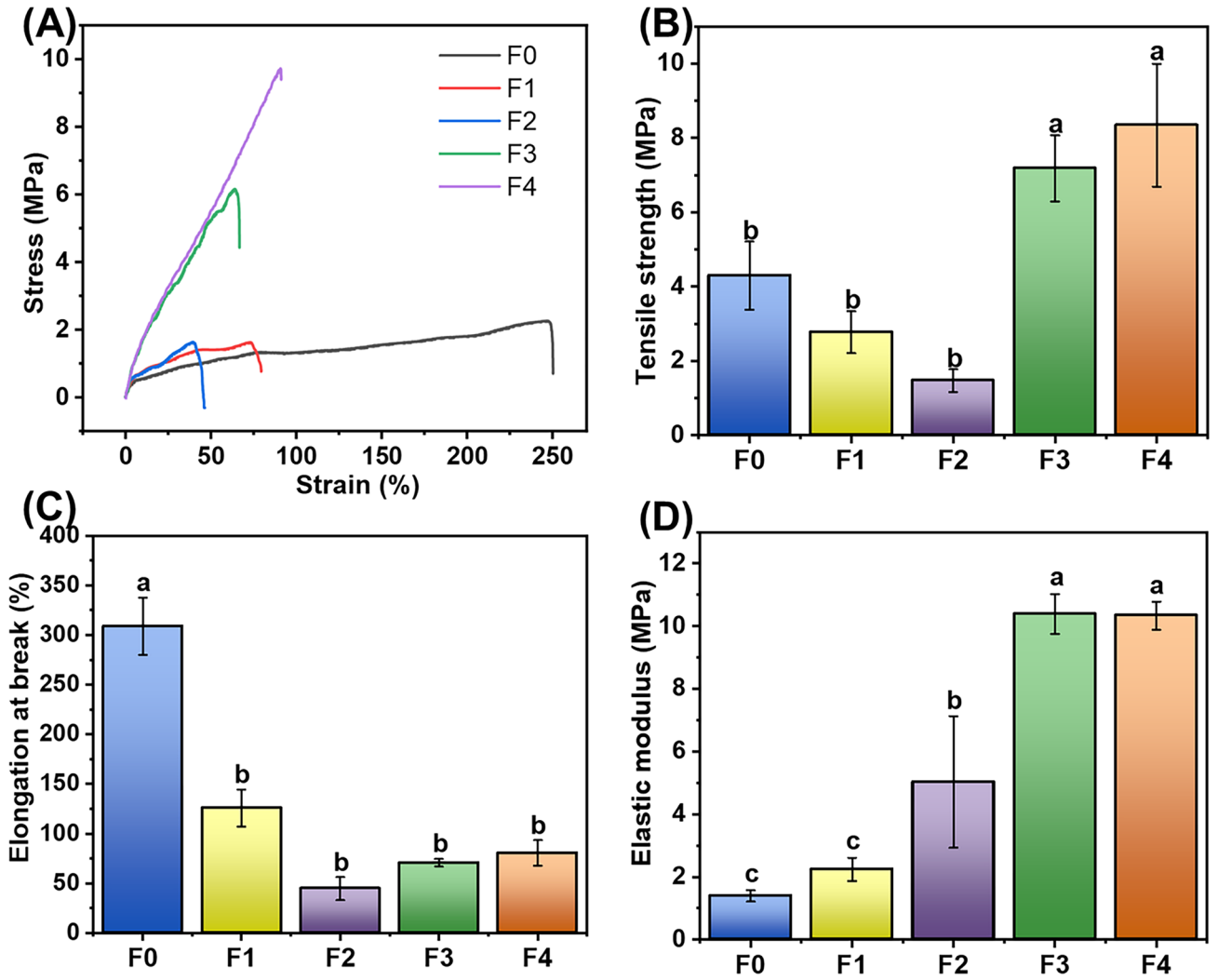


**Fig. 5** Mechanical performances of F0-F4 nanofibers: **a** stress–strain graphs, **b** tensile strength, **c** elongation at break, and **d** modulus of elasticity (different letters indicate significant differences between groups, $P < 0.05$)

in elongation at break occurred for the F3 and F4 nanofibers, but the tensile strength increased by about 40.25–48.56%, respectively, compared to the F0 nanofibers, and the modulus of elasticity increased from 1.39 ± 0.18 MPa (F0) to 10.38 ± 0.64 MPa (F3) and 10.34 ± 0.45 MPa (F4), respectively. This change could be attributed to the addition of nHA particles, which promoted the crystallization of PCL molecules, which enhanced the stiffness and strength of the fibers and made it difficult for them to undergo plastic denaturation, leading to a decrease in the elongation at break. The diameter of nHA particles is usually in the range of tens of nanometers, which has a large specific surface area, and a tighter interface can be formed between nanoparticles and polymer molecules to further enhance the mechanical properties of the nanofibers, which is consistent with previous studies [56]. The composite fibrous membrane F4 has excellent mechanical properties and can be used to support cell attachment and promote cell proliferation for restoration after periodontitis treatment.

## In vitro degradability

An ideal nanofiber implant membrane should have good biodegradable properties for load transfer for bone tissue regeneration. The amount of fibrous film loss over a period of one month was examined, and the results are shown in Fig. 6.

The results show that the nanofiber membranes degraded over time. As can be seen in Fig. 6a, the F0 nanofibers showed a very slow degradation throughout the one-month period, with the weight loss of the F1 ~ F4 nanofiber membranes on day 10 being 15.51 ± 3.11%, 20.47 ± 4.13%, 5.67 ± 2.16%, and 9.99 ± 1.07%, respectively. This initial weight loss has a close relationship with the incorporation of the hydrophilic drug and polymer.

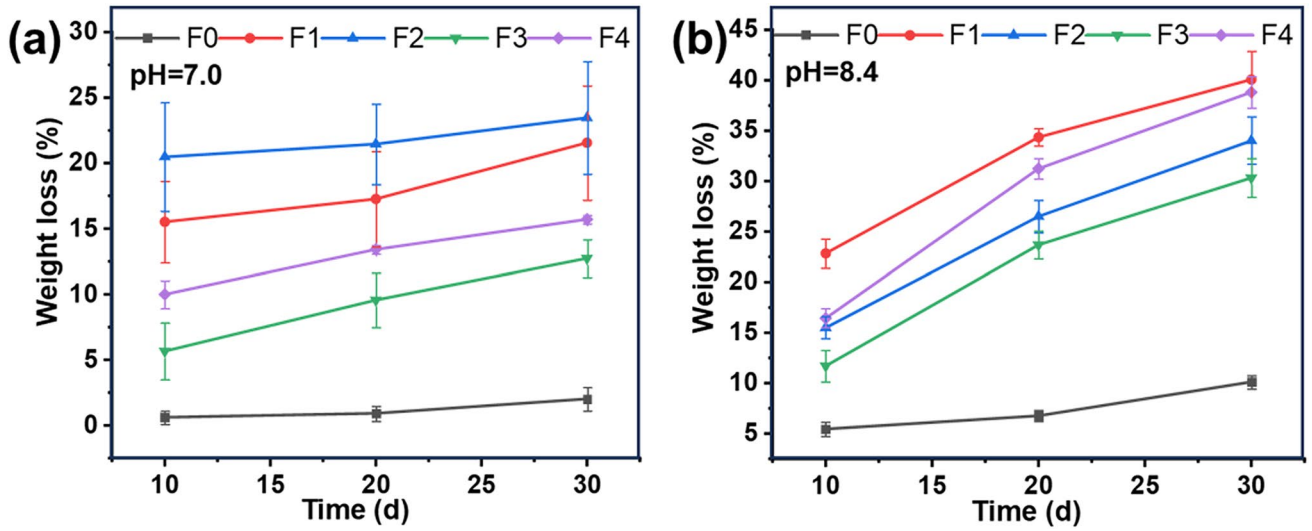


**Fig. 6** In vitro degradation of fibrous membranes: **a** degradation behavior in a neutral environment (pH = 7.0), and **b** degradation behavior in an alkaline environment (pH = 8.4)

When fibrous membranes are placed in a liquid medium, the highly hydrophilic polymer PVP on the surface first absorbs water molecules from the environment and undergoes hydrolysis reactions, prompting the gradual release of drug molecules from the carrier, and the fiber membranes show a surface erosion degradation pattern, which leads to a large weight loss of the fiber membranes. In addition, randomly distributed nanofibers show a disordered distribution, and the intertwining of fibers can form more network structures, which can also promote the degradation of the fiber membranes in a certain range [57]. The degradation results of the nanofiber membranes tested in this study in an alkaline environment are shown in Fig. 6b, and it can be seen that the degradation rate of the fiber membranes in the alkaline environment is greater than that in a neutral environment. The reason may be that the ester bond in the PCL molecules of the filament-forming matrix is easily hydrolyzed in an alkaline environment, which accelerates the degradation rate of the fiber membranes to some extent. Secondly, changes in the pH of the medium environment may also lead to changes in the physical and chemical properties of the fiber membranes, which affect the degradation rate of their material.

It should not be overlooked that maintaining the structure of the fibrous scaffold during the initial degradation phase has a crucial role in the release of the drug. During the experimental process, it was found that the fibrous membranes maintained their scaffold structure during the first ten days of degradation, and no scaffold fracture, collapse, or unformed state occurred; thus, the initial stage of degradation exerted little effect on the drug release process.

## In vitro drug release profile

The maximum UV absorbance is $\lambda_{max} = 260$ nm for the model drug KET, the equation of the calibration curve is $A = 0.06514\ C + 0.00665$ ($R^2 = 0.9996$), while the maximum UV absorbance is $\lambda_{max} = 320$ nm for MET, and the equation of the calibration curve is $A = 0.05354\ C + 0.00998$ ($R^2 = 0.9999$), where $C$ is the drug concentration (μg/mL) and $A$ is the absorbance. In vitro dissolution experiments were performed on the uniaxial F1 and F2 fibers and the tertiary juxtaposed F4 fibers, and the results are shown in Fig. 7.

Figure 7a shows the drug release profiles of the three types of fibers over 48 h. The release performance for the first 60 min is shown in Fig. 7b. In the first half hour, the F1 nanofibers released 30.51% ± 9.12% of KET, the F2 nanofibers released 78.63% ± 8.34% of MET, while the composite F4 nanofibers released 55.22% ± 1.47% of KET and 24.97% ± 1.53% of MET; the amounts of drug effectively released into the medium at 60 min were 47.40% ± 11.3 (F1), 94.7% ± 1.51% (F2), 82.83% ± 2.91% (F4-KET), and 50.86% ± 2.51% (F4-MET). The drug KET had a faster release profile from the Janus F4 nanofibers, while the drug MET exhibited a slower release effect from the F4 fibers due to its drug molecules being nested in the middle layer. Further, the time required to release 30% of each drug from each fiber was calculated, and the results are shown in Fig. 7c, where it can be seen that the homogeneous F2 fibers and the trilayer side-by-side F4 fibers could release 30% of MET and KET within 10 min. The time required to achieve 50% and 70% of drug release from each fiber is shown in Fig. 7d, where the time required to release 50% of the

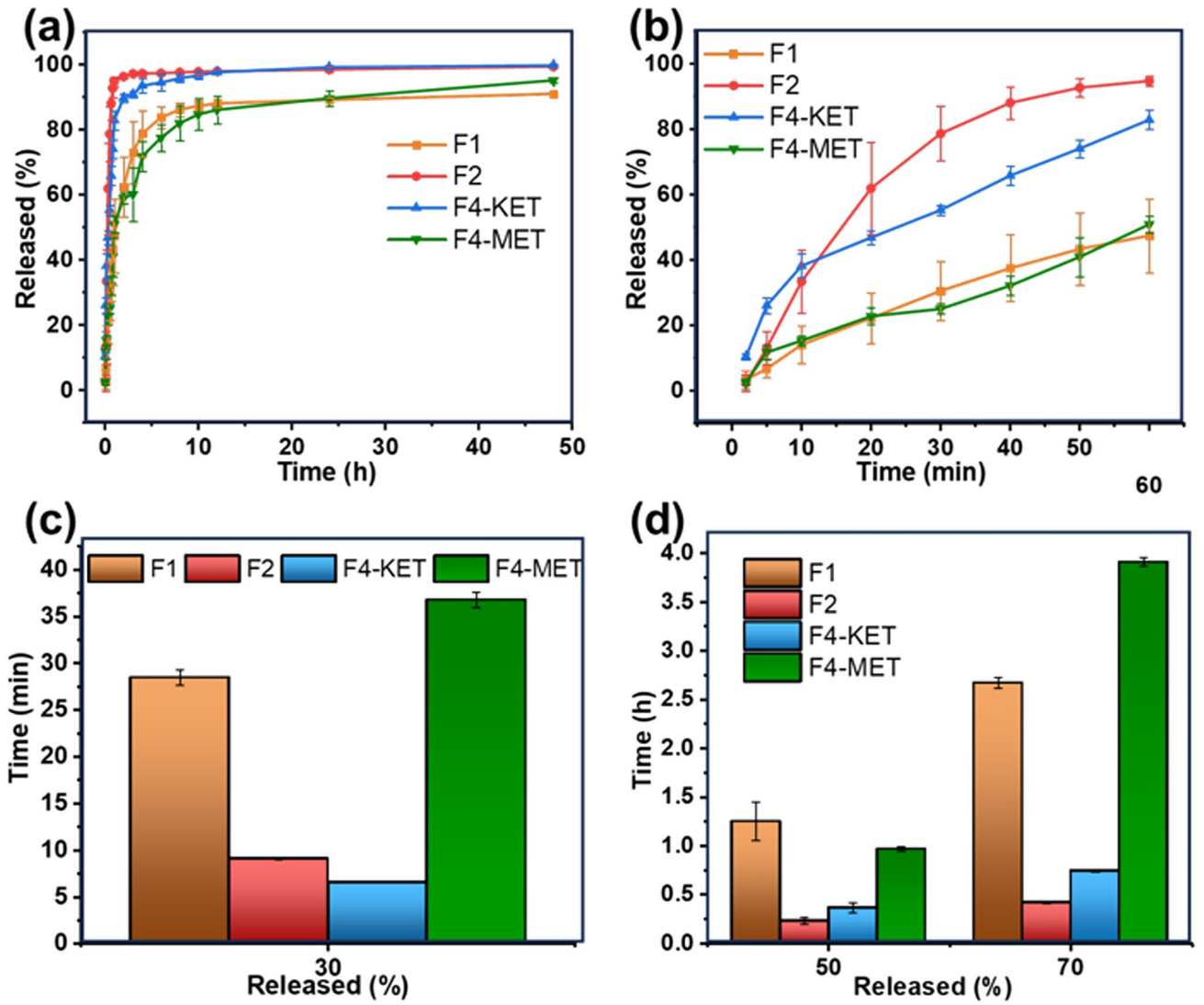


**Fig. 7** In vitro dissolution of fibrous membranes: **a** results in 48 h, **b** results in the first 60 min, **c** time required for F1, F2, and F4 nanofibers to achieve a percentage of 30% of drug release, and **d** time required for F1, F2, and F4 nanofibers to reach a percentage of 50–70% of drug release

drug from the F1, F2, and F4 fibers was 1.25 ± 0.20 h (F1), 0.23 ± 0.04 h (F2), 0.37 ± 0.05 h (F4-KET), and 0.98 ± 0.02 h (F4-MET), and the time taken to release 70% of the drug was 2.67 ± 0.06 h (F1), 0.42 ± 0.01 h (F2), 0.74 ± 0.01 h (F4-KET), and 3.91 ± 0.04 h (F4-MET). The F4 fibers are fibers with a trilayer nanostructure, whose outermost layer has a curved moon shape that facilitates the release of drugs. The middle layer consisting of PCL and MET is mostly covered by the outermost layer. Compared to the F2 nanofibers, the F4 nanofibers achieved good encapsulation of MET, which provided a smaller surface area to contact with the dissolution medium, thus allowing MET to have a longer time period for a better release effect than the F2 fibers. Thus, in general, the Janus F4 fibers were able to facilitate a faster KET release rate than the F1 fibers and a slower MET release rate than the F2 fibers. These drug release profiles would be very beneficial in reducing patients' pain and reducing the risk of inflammation and infection in the period of time shortly after periodontal surgery. Meanwhile, the extended release of the latter intermediate drug is, to a certain extent, conducive to maintaining a constant blood drug concentration to produce an effective antimicrobial effect. Moreover, both the drugs KET and MET presented an amorphous state in the Janus F4 fibers (the XRD patterns and FTIR spectra are given in the Fig. S7 and Fig. S8 in the Supplementary Materials, respectively), which is favorable for manipulating the guest drug's controllable release behaviors by the host polymeric carriers [58–60]. When the Peppas equation [61] was explored to treat the drug release data, both KET and MET were manipulated by the typical

Fickian mechanisms from samples F1, F2, F4-KET and F4-MET, which should be attributed to the insoluble PCL matrix and the amorphous state of drug molecules [37, 60] (The regressed equations and the SEM images of F4-MET after in vitro dissolution tests are included in Fig. S9).

## Antimicrobial properties

In this experiment, the antibacterial performance of the prepared fibrous implants F0 ~ F4 against *P.g* was investigated using the paper diffusion method. Figure 8a shows the results of the inhibition of bacterial growth by these materials, measured in terms of the mean zone of inhibition (in cm). It can be seen that the F2 and F4 nanofibers have significant inhibition circles, but the F0, F1, and F3 nanofibers show almost no inhibition circles. The size of the inhibition circle diameter was determined, and the results are shown in Fig. 8b. The diameter of the inhibition circle of the F2 nanofibers was 7.47 ± 0.34 cm, the diameter of the inhibition circle of the F4 nanofibers was 6.66 ± 0.83 cm, and the diameter of the inhibition circle of the F0, F1, and F3 nanofibers was 0. The bacterial activity statistics are shown in Fig. 8c; the bacterial activity of the F0 ~ F4 fibers was 100.29 ± 3.32%, 92.06 ± 5.56%, 21.01 ± 3.21%, 99.52 ± 7.12%, and 18.21 ± 2.44%, respectively. From the experimental results, it can be seen that the F2 and F4 nanofibers have larger inhibition circles and lower bacterial activity, which are mainly due to the fact that both nanofibers are loaded with the antimicrobial active substance MET. MET is a broad-spectrum antibiotic that interferes with the nucleic acid synthesis and metabolism of *P.g*, thereby inhibiting its growth and reproduction [62]. Therefore, these nanofiber films containing MET have good antimicrobial and biocompatible properties for antimicrobial treatment of periodontal tissues.

## Cellular activity

The results of the effect of each fibrous membrane on the cellular activity of HGFs measured over 7 days are shown in Fig. 9. It can be seen that on the third day, the cell viability values of the F1, F3, and F4 nanofibers showed an upward trend, indicating that cells responded positively to these fibrous membranes in the first period, which then stimulated

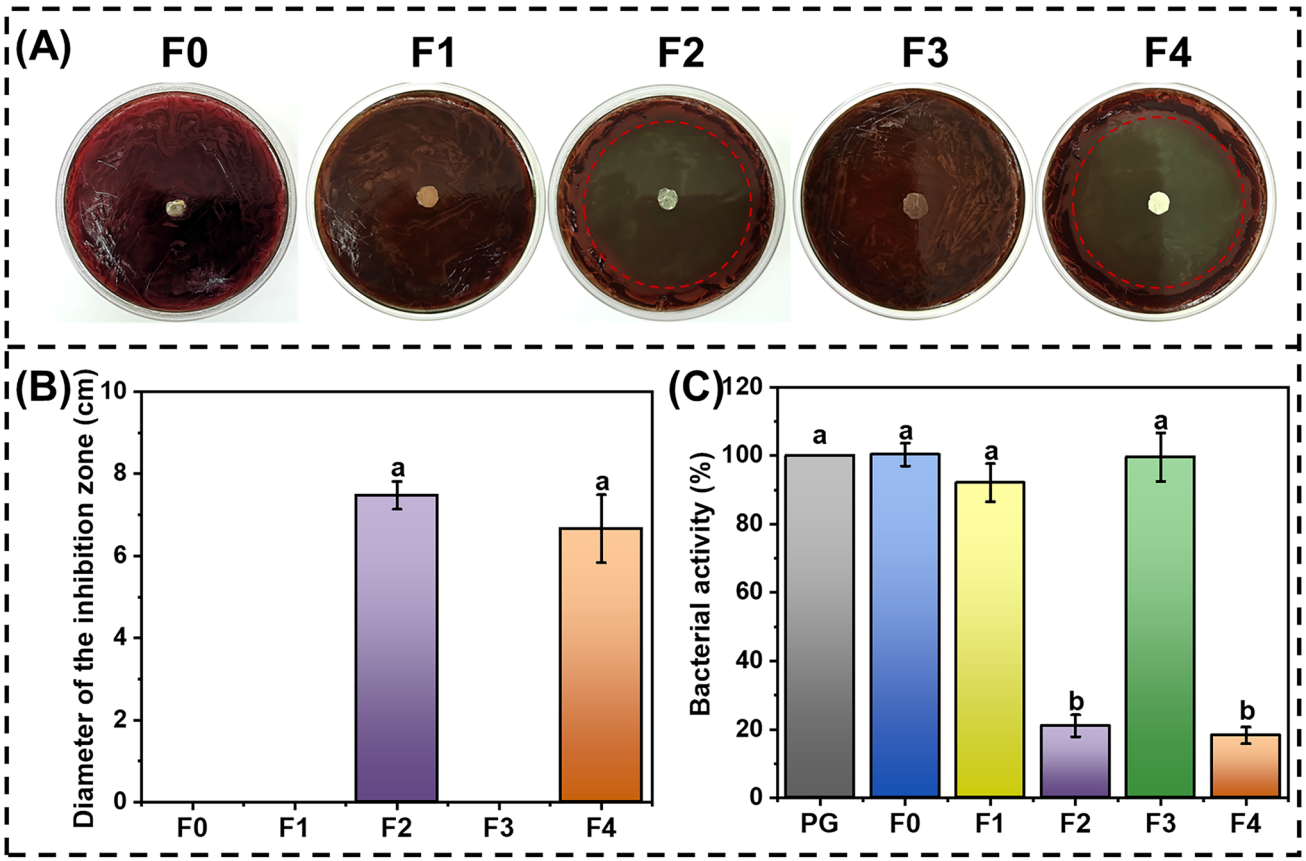


**Fig. 8** The antibacterial properties of fibrous membranes: **a** images of the inhibition circles of F0–F4 nanofibers against *P.g*., **b** statistical results of the diameter of the inhibition circles of F0–F4 nanofibers against *P.g*., and **c** statistics of the activity of F0 ~ F4 nanofibers against *P.g.* (different letters indicate significant differences between groups, $P < 0.05$)

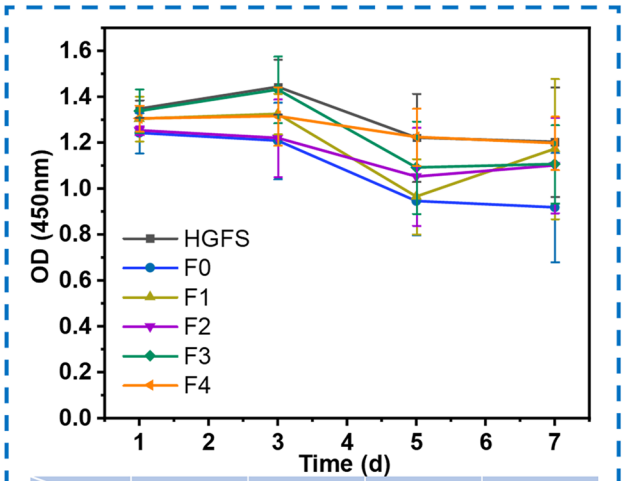


| Sample \ Day | Day 1 | Day 3 | Day 5 | Day 7 |
|---|---|---|---|---|
| HGFS | 1.35±0.04 | 1.44±0.12 | 1.22±0.19 | 1.20±0.24 |
| F0 | 1.24±0.09 | 1.21±0.17 | 0.95±0.15 | 0.92±0.24 |
| F1 | 1.30±0.10 | 1.33±0.09 | 0.97±0.16 | 1.17±0.31 |
| F2 | 1.25±0.02 | 1.22±0.17 | 1.05±0.21 | 1.10±0.21 |
| F3 | 1.34±0.10 | 1.43±0.15 | 1.09±0.20 | 1.11±0.17 |
| F4 | 1.31±0.06 | 1.32±0.13 | 1.22±0.12 | 1.20±0.12 |

**Fig. 9** Cell viability of fibrous films inoculated on human gingival fibroblasts within 7 days

the proliferation and metabolic activity of the cells. This led to an increase in OD values, indirectly giving a hint that the drugs KET and nHA did not produce toxicity to the cells at the designed concentrations, thus allowing the loading of KET and nHA particles to the outermost and innermost layers within the Janus F4 fibers for a direct contact with the periodontal tissue. On the fifth day, a decreasing trend in OD values was observed, presumably due to some natural maladaptation or damage similar to apoptosis and cell number saturation over time, which led to decreases in cell number and metabolic activity and a corresponding decrease in OD values. However, there were no significant differences compared to the blank control group ($1.22 \pm 0.19$). On the seventh day, the cell viability of the F4 nanofibers decreased the least, which could further indicate that this composite fibrous membrane has the least effect on cells, is less inhibitory or lethal to cells, and is also more favorable for cell proliferation and growth, thereby showing good biocompatibility for use in periodontitis treatment.

## Cytotoxicity

Based on the CCK-8 assay to assess the ability for cell proliferation, the effects of the fibrous implants on the proliferation of HGF cells were investigated via two methods: co-culture of the fiber scaffolds with cells and adhesion of cells to the fiber scaffolds. The results of cell staining are shown in Fig. 10, both for the live/dead staining of cells co-cultured with the materials (Fig. 10a–f) and for the live/dead staining of cells adhered to the materials (Fig. 10g–l). We observed that cells tended to align along the orientation of the fibers, and HGFs cells cultured on the F0 – F4 scaffolds showed good biocompatibility; no significant differences between the scaffolds were observed. The number of living cells was counted, and the results were shown in Fig. 11.

It can be seen that the F1–F3 fiber membranes are slightly toxic to cells at lower drug concentrations, and the amount of drug loaded in the F4 nanofibers is the sum of the drug loading of the former three nanofibers; at this high concentration, the F4 nanofibers do not exhibit stronger cytotoxicity. These results indicate that in the Janus F4 nanofibers, an active substance can be uniformly distributed in the nanofibers, which also helps the drug to be safely and appropriately released to the periodontal lesion site, resulting in a better therapeutic effect.

## Cell proliferation and adhesion

The adhesion effect of HGFs on the nanofibrous membranes is shown in Fig. 12. From the results, it can be seen that the fibroblasts grown on the fibrous scaffolds all maintained their normal morphology, and these cells grew randomly into polygonal shapes according to the multiple orientations of the different fibers. All scaffolds were able to support cell growth, and no significant differences were observed between scaffolds. The adhesion and proliferation properties of fibroblasts are important, especially in severe periodontitis with losses of gingival tissue and alveolar bone, and it is observed that the nanofibers tested in this study have good biocompatibility and can promote cell adhesion and cell growth.

## Anti-inflammatory properties

In this study, fluorescence signals were detected using a real-time PCR instrument, and the relative expression of IL-6, OPG, and the reference genes in the samples was calculated based on the intensity of the fluorescence signals. The $2^{-\Delta\Delta CT}$ method was used to calculate the relative expression of the genes, and the quantitative PCR primer sequences are shown in Table 2.

The m-RNA expression of the F0–F4 nanofibers was assessed via RT-qPCR using HGFs, and the results after 24 h of co-culture of the materials with the cells are shown in Fig. 13a. From the results, it can be seen that the expression levels of the F1 and F4 nanofibers tested for cytokines were reduced, showing that the materials themselves do not cause an increase in the expression of inflammatory factors. This

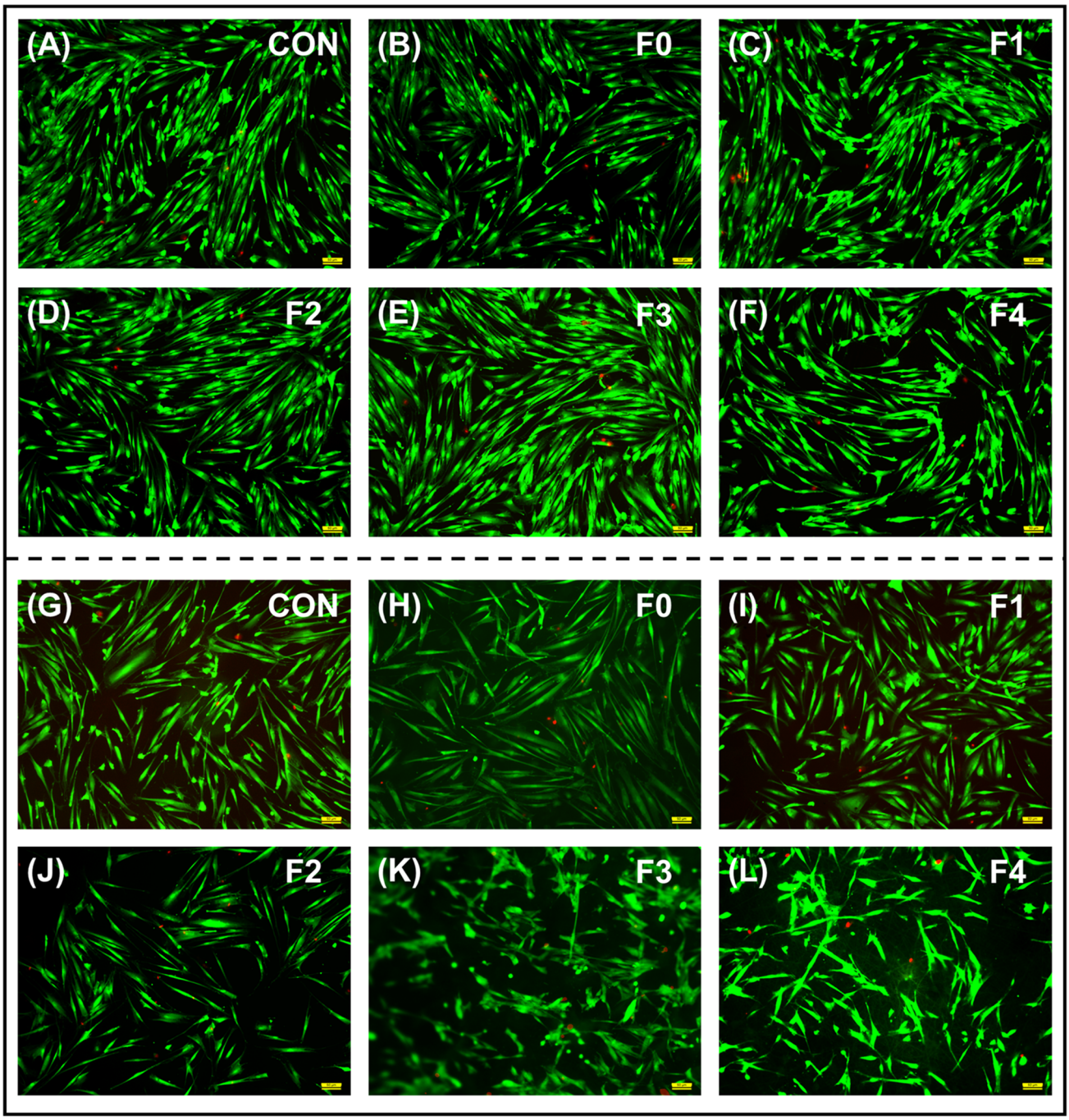


**Fig. 10** Fluorescence schematic of live/dead staining of HGFs on nanofibers: **a**–**f** live/dead staining of cells co-cultured with the material, and **g**–**l** live/dead staining of cells adhered to the material (live cells are stained green, dead cells are stained red, and all images are at a scale of 50 μm)

result may be due to the fact that both the F1 and F4 nanofibers are loaded with the active substance KET, a non-steroidal anti-inflammatory drug that reduces the synthesis of prostaglandins, which are capable of inducing inflammatory responses by inhibiting the activity of COX [63]. Secondly, when inflammation occurs in periodontal tissues, leukocytes will accumulate to the inflammation site and participate in the process of inflammatory reaction; at that time, KET can also inhibit the migration of leukocytes and reduce their aggregation, thus reducing the inflammatory reaction. When an inflammatory response is generated, the production of oxygen free radicals subsequently increases, and KET can reduce the extent of the inflammatory response by inhibiting the production of oxygen free radicals. In addition, KET can

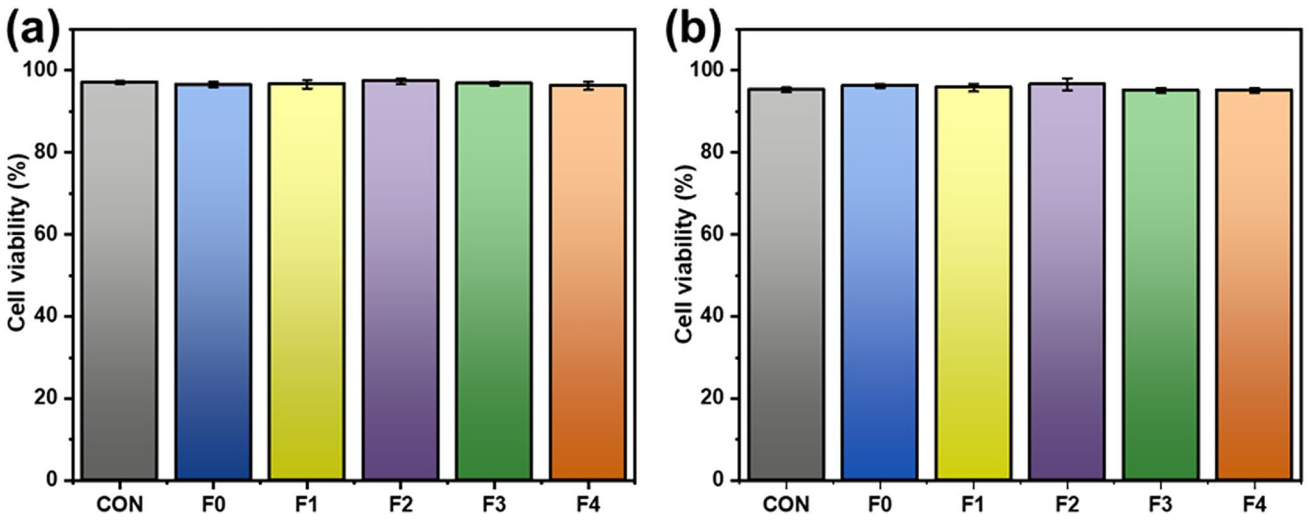


**Fig. 11** Cell viability statistics: **a** Percentage of living cells co-cultured with the material, and **b** The percentage of living cells that adhere to the material

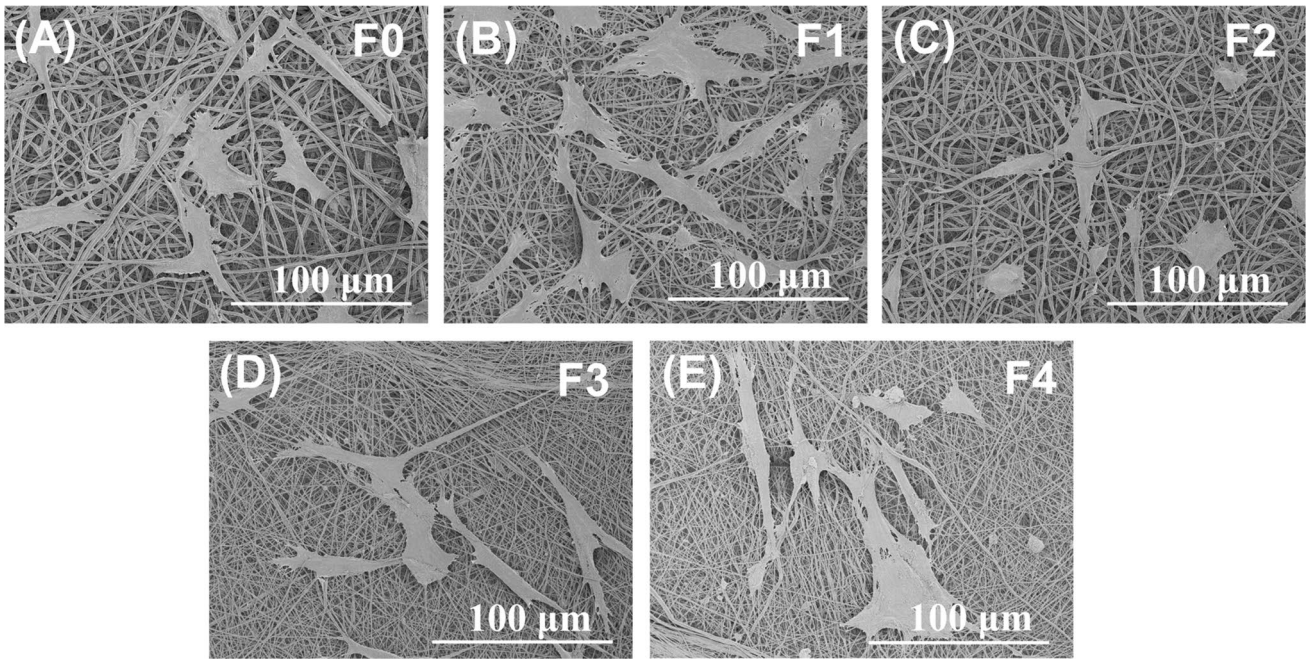


**Fig. 12** SEM images of cell growth on fibrous scaffolds

inhibit platelet aggregation and, thus, reduce the inflammatory response caused by platelet aggregation.

Lipopolysaccharide (LPS) is mainly found in the cell wall of Gram-negative bacteria. In the presence of an infection, LPS can trigger an inflammatory response in the body, leading to a massive release of cytokines [64]. Therefore, in this study, the mRNA levels of IL-6 in the F0, F1, and F4 nanofibers were evaluated via qPCR after these materials were co-cultured with HFG cells for 24 h. These cells were stimulated with 5 μg/mL of Pg LPS, and changes in the expression of the inflammatory factor IL-6 were detected via qPCR; the results are shown in Fig. 13b. The F1 and F4 nanofibers significantly down-regulated the LPS-induced IL6 mRNA expression, whereas the F0 nanofibers did not, and the result of the F4 nanofibers was significantly different from the control group, indicating that the tertiary juxtaposed composite F4 nanofibers could contribute to a reduction in the inflammatory response of organisms.

**Table 2** Gene primer sequences

| Gene name | Primer identification | Primer sequences |
|---|---|---|
| human IL-6 | M0007f | 5' GCA CCT CAG ATT GTT GTT G 3' |
| | M0007r | 5' AAA TAG TGT CCT AAC GCT CAT AC 3' |
| human OPG | M1224f | 5' AAC CCC AGA GCG AAA TAC A 3' |
| | M1224r | 5' TTA GCA GGA GAC CAA AGA CAC T 3' |

## Osteogenic properties

In addition to the inflammatory response caused by oral pathogens, re-absorption of alveolar bone is a fundamental feature of periodontitis. Therefore, suppression of inflammation and promotion of bone tissue growth are keys to the treatment of periodontitis. In this study, the F0, F3, and F4 nanofibers were selected for in vitro osteogenic property testing, mainly because both F3 and F4 nanofibers are loaded with nHA particles. The nHA chemical composition is similar to the main components of natural bone tissue, which can promote the proliferation and differentiation of osteoblasts, thus promoting bone tissue regeneration, which is essential for alveolar bone healing and periodontal regeneration [5]. The osteogenic gene selected for this study was OPG, whose main role is to inhibit the effect of bone resorption and, thus, maintain bone homeostasis. After co-culturing the materials and cells for 24 h, the expression of the osteogenic factor OPG was detected via qPCR, and the results are shown in Fig. 14. As expected, the F3 and F4 nanofibers caused an increase in OPG expression, while the F0 nanofibers did not, and it can be seen that the composite F4 nanofibers can be used to repair bone defects. In periodontitis treatment, the F4 nanofibers can be used as a bioactive scaffold for bone tissues, with good biocompatibility with the surrounding tissues of teeth, which can be absorbed and metabolized by cells in organisms, releasing calcium and phosphorus plasmas that are beneficial for bone tissue regeneration and further promoting bone tissue formation without causing an immune response. In addition, the extracellular matrix-like morphology of these nanofibers can provide a suitable

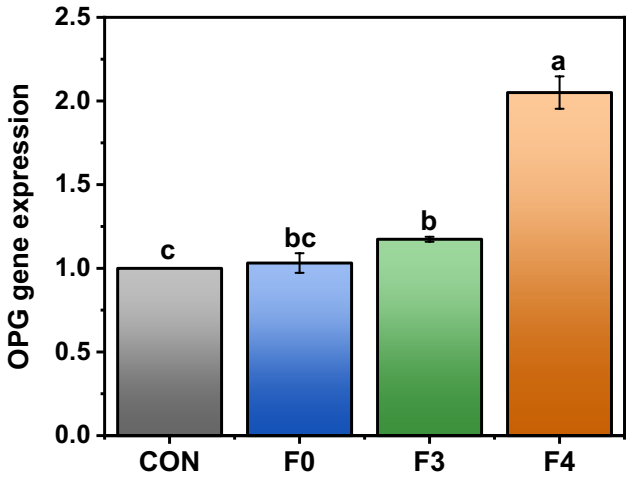


**Fig. 14** Representation of the expression of the osteogenic gene OPG detected via qPCR for F0, F3, and F4 fibers after 24 h of co-culturing these materials with cells (different letters indicate significant differences between groups, $P < 0.05$)

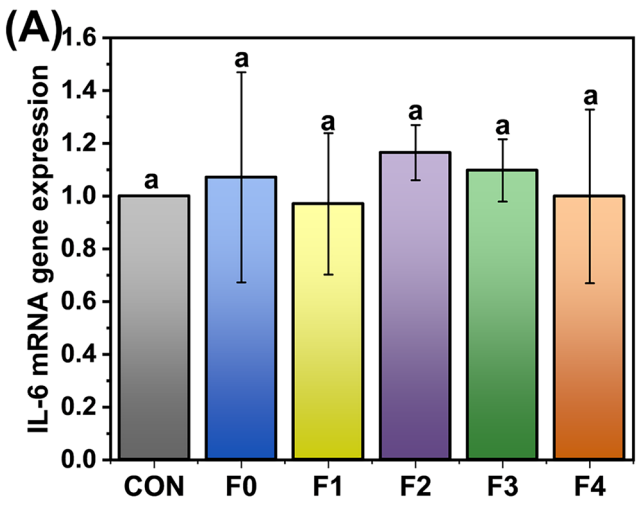


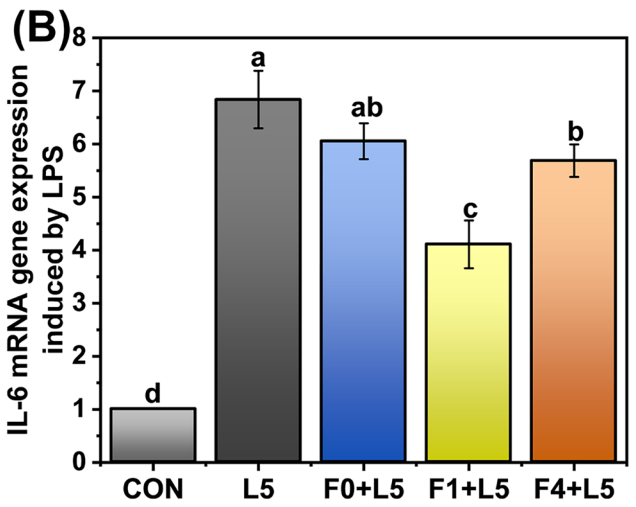


**Fig. 13** In vitro anti-inflammatory gene expression after 24 h of fiber–cell co-culture: **a** expression of inflammatory factor IL-6 detected via qPCR, and **b** change in expression of inflammatory factor IL-6 detected via qPCR after stimulation of cells with 5 μg/mL of Pg LPS (different letters indicate significant differences between groups, $P < 0.05$)

environment for cell adhesion, thus promoting the attachment and growth of bone cells and further maintaining the stable state of bones by promoting the production and maturation of osteoblasts and increasing the expression of the osteogenic gene OPG.

## Conclusions

In this study, complex functional fibrous implantable membranes with synergistic multi-drug properties were prepared using a multi-fluid electrospinning technology. In terms of the target functional application of these materials, the designed and prepared trilayer eccentric side-by-side composite structural nanomaterials enhanced the rapid release of poorly water-soluble drugs, and achieved the synergistic effects of anti-inflammation, antibacterial activity, and tissue growth promotion, which could achieve an efficient, safe, convenient, and comprehensive cure for periodontitis. The Janus fiber-based process–structure–performance relationship was explored.

Along this proof-of-concept investigation about generating eccentric and side-by-side three-layer composite nanofiber implanted membranes through a one-step method, there are many new possibilities for further developing novel multi-functional advanced fibrous nanomaterials. In terms of the targeted biomedical functional applications, the prepared tertiary composite structural nanomaterials are anticipated to solve the compatibility of drugs and organic solvents, enhance the solubility of insoluble drugs, promote the rapid release of drugs with poor water solubility and realize the synergistic effect of multi-drugs. Because of the high popularity of complex nanostructures and nano devices in this nano era and the unique property of tri-layer side-by-side structure for conceiving functional materials, it is expected to expand the capability of electrospinning in creating novel nanofibers and to support a research platform for biomedical and nanoscience developments. Meanwhile, there are a series of electrohydrodynamic scientific issues waited to be discerned about how to keep the three working fluids move under the electric field in a matched manner, by which the integrated three-chamber structure of the nanofibers can be ensured.

**Supplementary Information** The online version contains supplementary material available at https://doi.org/10.1007/s42765-024-00397-6.

**Acknowledgements** The study is financially supported by the Medical-Engineering Cross Project between University of Shanghai for Science and technology and Shanghai Jiaotong University (No. 202130071), and the Shanghai Industrial Collaboration Project (HCXBCY-2023-042 and XTCX-KJ-2023-44).

**Data availability** The data supporting the findings of this manuscript are available from the corresponding authors upon reasonable request.

## Declarations

**Conflict of interest** YL is presently an editorial board member for Advanced Fiber Materials. He was not involved in the editorial review or the decision to publish this article. All authors declare that there are no competing interests.

## References

1. Pedersen T, Krakenes J, Loes S. Multiple brain abscesses and ventriculitis secondary to chronic periodontitis. *Clin Case Rep*. **2020**;*8*:3612–3.
2. Rahimi A, Afshari Z. Periodontitis and cardiovascular disease: a literature review. *ARYA Atheroscler*. **2021**;*17*:1–8.
3. Sharma N, Durge KJ, Bajaj P, Kale B, Borle A. Periodontitis and diabetes mellitus-a two way relationship. *J Res Med Dent Sci*. **2011**;*10*:194–7.
4. Newman KL, Kamada N. Pathogenic associations between oral and gastrointestinal diseases. *Trends Mol Med*. **2022**;*28*:1030–9.
5. Andrei V, Andrei S, Gal AF, Rus V, Gherman L-M, Boșca BA, Niculae M, Barabas R, Cadar O, Dinte E, Muntean D-M, Peștean CP, Rotar H, Boca A, Chiș A, Tăut M, Candrea S, Ilea A. Immunomodulatory effect of novel electrospun nanofibers loaded with doxycycline as an adjuvant treatment in periodontitis. *Pharmaceutics*. **2023**;*15*:707.
6. Ray RR. Periodontitis: an oral disease with severe consequences. *Appl Biochem Biotechnol*. **2023**;*195*:17–32.
7. Xu B, Han YW. Oral bacteria, oral health, and adverse pregnancy outcomes. *Periodontol*. **2000**;*2022*(89):181–9.
8. Williams RC. Periodontal disease. *N Engl J Med*. **1990**;*322*:373–82.
9. Petrescu N, Crisan B, Aghiorghiesei O, Sarosi C, Mirica IC, Lucaciu O, Iușan SAL, Dirzu N, Apostu D. Gradual drug release membranes and films used for the treatment of periodontal disease. *Membranes*. **2022**;*12*:895.
10. Yamazaki M, Yamazaki K, Baba Y, Ito H, Loos BG, Takahashi K. The stages and grades of periodontitis are risk indicators for peri-implant diseases-a long-term retrospective study. *J Pers Med*. **2022**;*12*:1723.
11. Li J, Qu X, Liu L, Li L, Hua Y, Zhang J, Ishida M, Yoshida N, Tabata A, Sougawa N, Ito E, Mochizuki-Oda N, Harada A, Kawamura T, Matsuura R, Wang Y, Morishima K, Miyagawa S, Sawa Y. Developing thick cardiac tissue with a multilayer fiber sheet for treating myocardial infarction. *Adv Fiber Mater*. **2023**;*5*:1905–18.
12. Chen G, Xu S, Zhou Q, Zhang Y, Song Y, Mi J, Liu Y, Hou K, Pan J. Temperature-gated light-guiding hydrogel fiber for thermoregulation during optogenetic neuromodulation. *Adv Fiber Mater*. **2023**;*5*:968–78.
13. Liu J, Cui T, Xu X, Du Y, Wang L, Chen S, Pang J. Robust alcohol soluble polyurethane/chitosan/silk sericin (APU/CS/SS) nanofiber scaffolds toward artificial skin extracellular matrices via microfluidic blow-spinning. *Adv Fiber Mater*. **2023**;*5*:349–61.
14. Yu D-G, Zhao P. The key elements for biomolecules to biomaterials and to bioapplications. *Biomolecules*. **2022**;*12*:1234.
15. Zong D, Zhang X, Yin X, Wang F, Yu J, Zhang S, Ding B. Electrospun fibrous sponges: principle, fabrication, and applications. *Adv Fiber Mater*. **2022**;*4*:1434–62.
16. Chen Y, Dong X, Shafiq M, Myles G, Radacsi N, Mo X. Recent advancements on three-dimensional electrospun nanofiber scaffolds for tissue engineering. *Adv Fiber Mater*. **2022**;*4*:959–86.

17. Li L, Hao R, Qin J, Song J, Chen X, Rao F, Zhai J, Zhao Y, Zhang L, Xue J. Electrospun fibers control drug delivery for tissue regeneration and cancer therapy. *Adv Fiber Mater*. **2022**;*4*:1375–413.
18. Hofer U. Fusobacterium orchestrates oral biofilms. *Nat Rev Microbiol*. **2022**;*20*:576.
19. Porter JR, Henson A, Popat KC. Biodegradable poly(epsilon-caprolactone) nanowires for bone tissue engineering applications. *Biomaterials*. **2009**;*30*:780–8.
20. Duan H, Chen H, Qi C, Lv F, Wang J, Liu Y, Liu Z, Liu Y. A novel electrospun nanofiber system with PEGylated paclitaxel nanocrystals enhancing the transmucus permeability and in situ retention for an efficient cervicovaginal cancer therapy. *Int J Pharm*. **2024**;*650*: 123660.
21. Huang X, Jiang W, Zhou J, Yu DG, Liu H. The applications of ferulic-acid-loaded fibrous films for fruit preservation. *Polymers*. **2022**;*14*:4947.
22. Li J, Du Q, Wan J, Yu DG, Tan F, Yang X. Improved synergistic anticancer action of quercetin and tamoxifen citrate supported by an electrospun complex nanostructure. *Mater Des*. **2024**;*238*: 112657.
23. Yu DG, Zhou J. Electrospun multi-chamber nanostructures for sustainable biobased chemical nanofibers. *Next Mater*. **2024**;*1*:119. https://doi.org/10.1016/j.nxmate.2024.100119.
24. Chen X, Liu Y, Liu P. Electrospun core-sheath nanofibers with a cellulose acetate coating for the synergistic release of zinc ion and drugs. *Mol Pharm*. **2024**;*21*:173–82.
25. Fu L, Feng Q, Chen Y, Fu J, Zhou X, He C. Nanofibers for the immunoregulation in biomedical applications. *Adv Fiber Mater*. **2022**;*4*:1334–56.
26. Deng YK, Zhu MM, Lu T, Fan QW, Ma WJ, Zhang XL, Chen L, Min HH, Xiong RH, Huang CB. Hierarchical fiber with granular-convex structure for highly efficient PM25 capture. *Sep Purif Technol*. **2023**;*304*:122235.
27. Wang M, Hou J, Yu D-G, Li S, Zhu J, Chen Z. Electrospun tri-layer nanodepots for sustained release of acyclovir. *J Alloys Compd*. **2020**;*846*: 156471.
28. Li D, Yue G, Li S, Liu J, Li H, Gao Y, Liu J, Hou L, Liu X, Cui Z, Wang N, Bai J, Zhao Y. Fabrication and applications of multifluidic electrospinning multi-structure hollow and core–shell nanofibers. *Engineering*. **2022**;*13*:116–27.
29. Yao Z-C, Zhang C, Xing Z, Ahmad Z, Ding Q, Chang M-W. Controlled engineering of multifunctional porous structures using tri-needle co-axial electrohydrodynamic flow and sacrificial media. *Chem Eng J*. **2022**;*429*: 132221.
30. Jiao Y, Li X, Chen J, Li C, Liu L, Liu X, Wang F, Chen G, Wang L. Constructing nanoscale topology on the surface of microfibers inhibits fibroblast fibrosis. *Adv Fiber Mater*. **2022**;*4*:1219–32.
31. Yang Y, Du Y, Zhang J, Zhang H, Guo B. Structural and functional design of electrospun nanofibers for hemostasis and wound healing. *Adv Fiber Mater*. **2022**;*4*:1027–57.
32. Lu H, Zhao Y, Qin S, Zhang Y, Liu J, Zhang J, Feng C, Zhao W. Fluorine substitution tunes the nanofiber chirality of supramolecular hydrogels to promote cell adhesion and proliferation. *Adv Fiber Mater*. **2023**;*5*:377–87.
33. Xing C, Zhu H, Dou X, Gao L, Baddi S, Zou Y, Zhao C, Peng Y, Fang Y, Feng CL. Infected diabetic wound regeneration using peptide-modified chiral dressing to target revascularization. *ACS Nano*. **2023**;*17*:6275–91.
34. Kang S, Hou S, Chen X, Yu DG, Wang L, Li XR, Williams G. Energy-saving electrospinning with a concentric Teflon-core rod spinneret to create medicated nanofibers. *Polymers*. **2020**;*12*:2421.
35. Zhou J, Yi T, Zhang Z, Yu D-G, Liu P, Wang L, Zhu Y. Electrospun Janus core (ethyl cellulose//polyethylene oxide) @ shell (hydroxypropyl methyl cellulose acetate succinate) hybrids for an enhanced colon-targeted prolonged drug absorbance. *Adv Compos Hybrid Mater*. **2023**;*6*:189.
36. Wang Y, Yu DG, Liu Y, Liu YN. Progress of electrospun nanofibrous carriers for modifications to drug release profiles. *J Funct Biomater*. **2022**;*13*:289.
37. He H, Wu M, Zhu J, Yang Y, Ge R, Yu D-G. Engineered spindles of little molecules around electrospun nanofibers for biphasic drug release. *Adv Fiber Mater*. **2022**;*4*:305–17.
38. Dos Santos DM, Chagas PAM, Leite IS, Inada NM, de Annunzio SR, Fontana CR, Campana-Filho SP, Correa DS. Core-sheath nanostructured chitosan-based nonwovens as a potential drug delivery system for periodontitis treatment. *Int J Biol Macromol*. **2020**;*142*:521–34.
39. Mirzaeei S, Moghadam F, Asare-Addo K, Nokhodchi A. Design of a nanofibrous guided tissue regeneration carrier as a potential drug delivery system for tetracycline hydrochloride in the management of periodontitis. *J Drug Deliv Sci Technol*. **2022**;*75*: 103722.
40. Lu T, Cao WX, Liang HB, Deng YK, Zhang YY, Zhu MM, Ma WJ, Xiong RH, Huang CB. Blow-spun nanofibrous membrane for simultaneous treatment of emulsified oil/water mixtures, dyes, and bacteria. *Langmuir*. **2022**;*38*:15729–39.
41. Zhu J, Ye H, Deng D, Li J, Wu Y. Electrospun metformin-loaded polycaprolactone/chitosan nanofibrous membranes as promoting guided bone regeneration membranes: preparation and characterization of fibers, drug release, and osteogenic activity in vitro. *J Biomater Appl*. **2020**;*34*:1282–93.
42. Fraire JC, Shaabani E, Sharifiaghdam M, Rombaut M, Hinnekens C, Hua DW, Ramon J, Raes L, Bolea-Fernandez E, Brans T, Vanhaecke F, Borghgraef P, Huang CB, Sauvage F, Vanhaecke T, De Kock J, Xiong RH, De Smedt S, Braeckmans K. Light triggered nanoscale biolistics for efficient intracellular delivery of functional macromolecules in mammalian cells. *Nat Commun*. **1996**;*2022*:13.
43. Dos Santos DM, de Annunzio SR, Carmello JC, Pavarina AC, Fontana CR, Correa DS. Combining coaxial electrospinning and 3D printing: design of biodegradable bilayered membranes with dual drug delivery capability for periodontitis treatment. *ACS Appl Bio Mater*. **2022**;*5*:146–59.
44. Budai-Szűcs M, Ruggeri M, Faccendini A, Léber A, Rossi S, Varga G, Bonferoni MC, Vályi P, Burián K, Csányi E, Sandri G, Ferrari F. Electrospun scaffolds in periodontal wound healing. *Polymers*. **2021**;*13*:307.
45. Reise M, Kranz S, Guellmar A, Wyrwa R, Rosenbaum T, Weisser J, Jurke A, Schnabelrauch M, Heyder M, Watts DC, Sigusch BW. Coaxial electrospun nanofibers as drug delivery system for local treatment of periodontitis. *Dent Mater*. **2023**;*39*:132–9.
46. Ho M-H, Claudia JC, Tai W-C, Huang K-Y, Lai C-H, Chang C-H, Chang Y-C, Wu Y-C, Kuo MY-P, Chang P-C. The treatment response of barrier membrane with amoxicillin-loaded nanofibers in experimental periodontitis. *J Periodontol*. **2021**;*92*:886–95.
47. Bottino MC, Albuquerque MTP, Azabi A, Münchow EA, Spolnik KJ, Nör JE, Edwards PC. A novel patient-specific three-dimensional drug delivery construct for regenerative endodontics. *J Biomed Mater Res B Appl Biomater*. **2019**;*107*:1576–86.
48. Ma Y, Song J, Almassri HNS, Zhang D, Zhang T, Cheng Y, Wu X. Minocycline-loaded PLGA electrospun membrane prevents alveolar bone loss in experimental peridontitis. *Drug Deliv*. **2020**;*27*:151–60.
49. Batool F, Morand D-N, Thomas L, Bugueno IM, Aragon J, Irusta S, Keller L, Benkirane-Jessel N, Tenenbaum H, Huck O. Synthesis of a novel electrospun polycaprolactone scaffold functionalized with ibuprofen for periodontal regeneration: an in vitro and in vivo study. *Materials*. **2018**;*11*:580.
50. Xiong RH, Sauvage F, Fraire JC, Huang CB, De Smedt SC, Braeckmans K. Photothermal nanomaterial-mediated photoporation. *Acc Chem Res*. **2023**;*56*:631–43.
51. Nasajpour A, Ansari S, Rinoldi C, Rad AS, Aghaloo T, Shin SR, Mishra YK, Adelung R, Swieszkowski W, Annabi N,

Khademhosseini A, Moshaverinia A, Tamayol A. A multifunctional polymeric periodontal membrane with osteogenic and antibacterial characteristics. *Adv Funct Mater*. **2018**;*28*:1703437.
52. Andrei V, Fiț NI, Matei I, Barabás R, Bizo LA, Cadar O, Boșca BA, Farkas N-I, Marincaș L, Muntean D-M, Dinte E, Ilea A. In vitro antimicrobial effect of novel electrospun polylactic acid/hydroxyapatite nanofibres loaded with doxycycline. *Materials*. **2022**;*15*:6225.
53. Liu Z-Q, Shang L-L, Ge S-H. Immunomodulatory effect of dimethyloxallyl glycine/nanosilicates-loaded fibrous structure on periodontal bone remodeling. *J Dent Sci*. **2021**;*16*:937–47.
54. Zhao K, Lu Z-H, Zhao P, Kang S-X, Yang Y-Y, Yu D-G. Modified tri–axial electrospun functional core–shell nanofibrous membranes for natural photodegradation of antibiotics. *Chem Eng J*. **2021**;*425*: 131455.
55. Xiong RH, Hua DW, Van Hoeck J, Berdecka D, Léger L, De Munter S, Fraire JC, Raes L, Harizaj A, Sauvage F, Goetgeluk G, Pille M, Aalders J, Belza J, Van Acker T, Bolea-Fernandez E, Si T, Vanhaecke F, De Vos WH, Vandekerckhove B, van Hengel J, Raemdonck K, Huang CB, De Smedt SC, Braeckmans K. Photothermal nanofibres enable safe engineering of therapeutic cells. *Nat Nanotechnol*. **2021**;*16*:1281–91.
56. Alehosseini M, Golafshan N, Kharaziha M. Design and characterization of poly-ε-caprolactone electrospun fibers incorporated with α-TCP nanopowder as a potential guided bone regeneration membrane. *Mater Today: Proc*. **2018**;*5*:15783–9.
57. Xu X, Zhou Y, Zheng K, Li X, Li L, Xu Y. 3D polycaprolactone/gelatin-oriented electrospun scaffolds promote periodontal regeneration. *ACS Appl Mater Interf*. **2022**;*14*:46145–60.
58. Chen S, Zhou J, Fang B, Ying Y, Yu DG, He H. Three EHDA processes from a detachable spinneret for fabricating drug fast dissolution composites. *Macromol. Mater. Eng.* **2023**, 202300361.
59. Wang Y, Liu L, Zhu Y, Wang L, Yu DG, Liu L. Tri-layer core–shell fibers from coaxial electrospinning for a modified release of metronidazole. *Pharmaceutics*. **2023**;*15*:2561.
60. Zhou J, Dai Y, Fu J, Yan C, Yu DG, Yi T. Dual-step controlled release of berberine hydrochloride from the trans-scale hybrids of nanofibers and microparticles. *Biomolecules*. **2023**;*13*:1011.
61. Peppas NA. Analysis of Fickian and non-Fickian drug release from polymers. *Pharm Acta Helv*. **1985**;*60*:110–1.
62. Deepak A, Goyal AK, Rath G. Development and characterization of novel medicated nanofiber for the treatment of periodontitis. *AAPS PharmSciTech*. **2018**;*19*:3687–97.
63. Cekici A, Kantarci A, Hasturk H, Van Dyke TE. Inflammatory and immune pathways in the pathogenesis of periodontal disease. *Periodontol*. **2000**;*2014*(64):57–80.
64. Di Cristo F, Valentino A, De Luca I, Peluso G, Bonadies I, Calarco A, Di Salle A. PLA nanofibers for microenvironmental-responsive quercetin release in local periodontal treatment. *Molecules*. **2022**;*27*:2205.